HHS Public Access

Author manuscript

Neuron. Author manuscript; available in PMC 2018 October 11.

Published in final edited form as:

Neuron. 2017 October 11; 96(2): 355–372.e6. doi:10.1016/j.neuron.2017.09.041.

Amyloid Beta Peptides Block New Synapse Assembly by Nogo Receptor Mediated Inhibition of T-Type Calcium Channels

Yanjun Zhao[1], **Sivaprakash Sivaji**[1], **Michael C. Chiang**[1,4], **Haadi Ali**[1], **Monica Zukowski**[1], **Sareen Ali**[1], **Bryan Kennedy**[1], **Alex Sklyar**[1], **Alice Cheng**[1], **Zihan Guo**[1], **Alexander K. Reed**[1], **Ravindra Kodali**[2], **Jennifer Borowski**[1], **Georgia Frost**[1], **Patrick Beukema**[3,4], and **Zachary P. Wills**[1,4,‡]

[1]Department of Neurobiology, University of Pittsburgh, 200 Lothrop Street, Pittsburgh, PA 15213, USA

[2]Department of Structural Biology and Pittsburgh Institute for Neurodegenerative Diseases, University of Pittsburgh School of Medicine, Pittsburgh, PA 15213, USA

[3]Center for the Neural Basis of Cognition, Carnegie Mellon University, Pittsburgh, PA 15213, USA

[4]Center for Neuroscience, University of Pittsburgh, Pittsburgh, PA 15260, USA

SUMMARY

Compelling evidence links amyloid beta (Aβ) peptide accumulation in the brains of Alzheimer's disease (AD) patients with the emergence of learning and memory deficits; yet a clear understanding of the events that drive this synaptic pathology are lacking. We present evidence that neurons exposed to Aβ are unable to form new synapses, resulting in learning deficits *in vivo*. We demonstrate the Nogo receptor family (NgR1-3) act as Aβ receptors mediating an inhibition of synapse assembly, plasticity and learning. Live imaging studies reveal Aβ activates NgRs on the dendritic shaft of neurons triggering an inhibition of calcium signaling. We define T-type calcium channels as a target of Aβ-NgR signaling, mediating Aβ's inhibitory effects on calcium, synapse assembly, plasticity and learning. These studies highlight deficits in new synapse assembly as a potential initiator of cognitive pathology in AD, and pinpoint calcium dysregulation mediated by NgRs and T-type channels as key components.

[‡]To whom correspondence should be addressed: University of Pittsburgh, Department of Neurobiology, Room 1457, BST Building, 200 Lothrop Street, Pittsburgh, PA 15213, Phone: 412-624-9176, Fax 412-383-8663, zpwills@pitt.edu.

AUTHOR CONTRIBUTIONS

Y.Z. did electrophysiology experiments. S.S., H.A, S.A., A.S., A.C., A.R. and B.K did dendritic spine imaging and analysis studies. Z.G. did Abeta and ADDL binding and imaging experiments. R.K. did SEC, EM and HPLC experiments. Z.W., S.S. and A.C. did sensor imaging and analysis studies. M.Z. and Z.W. did NOR analysis. M.C. did ICV injections. P.B. wrote code for analyzing calcium imaging data. J.B., G.F. and S.S. did animal husbandry, genotyping and neuronal dissections. Z.W. conceived of experiments, oversaw execution of the project, contributed to interpretation of the data and wrote the manuscript. All authors provided comments and edits to produce the final version of the manuscript.

INTRODUCTION

Among the leading causes of death in the United States of America only Alzheimer's disease remains without treatments. Research has identified some primary culprits driving AD pathology, chief among them amyloid beta (Aβ) peptides (reviewed in Tanzi, 2005). However, a failure to understand the initiating events that drive AD pathogenesis limits the development of effective tools to reverse this disease.

Clinical observations suggest among the first AD symptoms is an impairment in learning (Buckner, 2004). In support of Aβ peptides driving this deficit, Aβ is the earliest known biomarker in AD patients (Jack et al., 2013). Further, genetic mutations resulting in Aβ overproduction lead to AD (Selkoe, 2001). Finally, Aβ peptides isolated from AD patients trigger synapse loss, reduce synaptic plasticity and compromise learning in rodents (Shankar et al., 2008). While it has been assumed Aβ acts by eliminating existing synapses, little work has validated this claim or explored whether Aβ might compromise new synapse assembly. Given emergent synapses are essential for new memory acquisition (Hayashi-Takagi et al., 2015), one might predict learning deficiencies in AD result from deficits in new synapse assembly.

Numerous features of brain circuits are altered during learning, including an increase in excitatory synapse size and changes in synaptic plasticity (Nabivi et al., 2014), including long-term potentiation (LTP). Consistent with Aβ compromising learning efficacy, neural circuits exposed to Aβ peptides show reductions in spine size and LTP (Walsh et al., 2002; Shankar et al., 2007). A critical intracellular mediator initiating synapse assembly, growth and plasticity is calcium (Lohmann et al., 2008; Yasuda et al., 2003); yet how alterations in calcium impact learning remains poorly understood.

Calcium dysregulation is a hallmark feature of AD (Bezprozvanny and Mattson, 2008). Elevated levels of serum calcium correlate with cognitive decline during aging and AD (Schram et al., 2007). Calcium imaging studies in AD mouse models or following Aβ exposure show populations of neurons that are aberrantly hyperactive or silent (Busche et al., 2012). Several receptors bind Aβ and contribute to aberrant calcium activity in neurons (reviewed in Jarosz-Griffiths et al., 2016); yet how these receptors function is unclear.

A central regulator restricting synapse assembly and plasticity is the Nogo receptor family (NgR1-3; Mironova and Giger, 2013). Blocking NgR signaling augments synaptic plasticity in numerous brain regions. Loss of the NgR family (NgR^{TKO}) increases excitatory synapse number in the hippocampus, triggered by new synapse assembly resulting from NgR loss on dendrites (Wills et al., 2012). NgR1 is known to bind Aβ, yet NgR's role in Aβ's synaptic pathologies remains unexamined (Park et al., 2006).

Nogo receptors restrict synaptogenesis via the GTPase RhoA and its downstream effector Rho Kinase (ROCK: Wills et al., 2012). ROCK inhibits cytoskeletal assembly via phosphorylation of numerous cytoskeletal substrates (Schmandke et al., 2007). While RhoA and ROCK are implicated in Aβ's synaptic pathologies, the Aβ receptors activating them and their cellular targets remain undefined. ROCK regulates numerous voltage-gated calcium channels (VGCC; Iftinca et al., 2007), suggesting ROCK might modulate calcium

signaling to mediate its effects on synaptic development. T-type calcium channels (CaV3.1-3.3) are expressed on pyramidal neurons and contribute to synaptic calcium signaling, making them compelling candidates for mediating NgR-ROCK-dependent synaptic biology (Magee et al., 1995; McKay et al., 2006).

In this study we sought to define the mechanism by which Aβ compromises learning. We determined Aβ inhibits new synapse assembly and identify the NgR family as mediating Aβ's inhibition of synaptogenesis and synaptic plasticity. Imaging studies pinpoint Aβ activates NgR-RhoA signaling on the dendritic shaft of hippocampal neurons, where it inhibits calcium signaling. Electrophysiology demonstrates T-type calcium channels are a target of Aβ-NgR signaling, mediating Aβ's inhibition of synapse development, plasticity and calcium signaling. *In vivo* studies reveal Aβ reduces spine number, T-type currents and new learning via the NgR family. This study highlights that deficits in new synapse assembly may contribute to learning difficulties emerging early in AD progression, and identifies NgRs and T-type calcium channels as key mediators.

RESULTS

ADDLs inhibit new spine assembly dependent on NgR1

Neurons exposed to Aβ peptides show reduced numbers of excitatory synapses (Shankar et al., 2007); however, whether synapse loss results from increased synapse elimination or decreased synapse addition has not been examined. To address this question we tracking dendritic spine addition and elimination in live imaging studies of hippocampal slice cultures following neuronal exposure to oligomeric preparations of Aβ peptides (ADDLs-amyloid beta-derived diffusible ligands). CA1 pyramidal neurons were biolistically labeled with venus GFP (vGFP) and primary apical dendrites were imaged every two days over a six-day period using confocal microscopy (Wills et al., 2012). ADDLs were prepared as outlined in Figure S1 (Nicoll et al., 2013). The concentration, size and oligomeric status of Aβ peptides were assessed by high-performance liquid chromatography (HPLC), size exclusion chromatography (SEC) and electron microscopy (EM) respectively (Figure S1). We find ~30% of our ADDL preparations run as oligomers at ~500 kDa, equivalent to ~100 Aβ peptide monomers (Nicoll et al., 2013).

Following exposure to ADDLs (150 nM) we observe a significant reduction in overall spine density in CA1 pyramidal neurons at both 48 and 96 hours (Figure 1A and B). Quantification of spine addition (green numbers) and elimination (red numbers) reveal ADDLs inhibit spine addition at both time points relative to controls, while spine elimination rates remained unaffected (Figure 1A, B). In contrast, monomeric Aβ peptides or a DMSO control have no effect on spine density (Figure S1E). These findings demonstrate ADDLs specifically inhibit new spine addition to reduce synapse number.

Given NgRs are known to restrict new spine addition (Wills et al., 2012), we considered whether NgRs mediate Aβ's inhibition of synapse assembly. Following biolistic introduction of a validated shRNAi targeting NgR1 in hippocampal slices, we find, consistent with previous work (Wills et al., 2012), that NgR1 loss increases spine density over a 48-hour period, an effect resulting from augmented spine addition (Figure 1C and D). Strikingly,

neurons lacking NgR1 still show an increase in spine density and spine addition after ADDL exposure over a 48-hour period, comparable to shNgR1 neurons alone. Spine elimination is unaffected in all conditions. These findings reveal NgR1 is required for Aβ's inhibition of new spine assembly.

NgRs and ROCK Mediate ADDL Inhibition of LTP

NgR signaling restricts learning and new spine assembly triggered during this process (Zemmar et al., 2014). To gain mechanistic insight into how NgRs function, we assessed LTP, a plasticity mechanism required for learning (Nabavi et al., 2014). Given AD is an aging-associated disease, we carried out studies in 6–10-month-old mice, the age at which LTP deficits first emerge in several AD mouse models (Oddo et al, 2003). In field excitatory postsynaptic current (fEPSCs) recordings of CA1 pyramidal neurons following high frequency stimulation of Schaffer collateral axons, we find animals lacking all three NgRs ($NgR1^{-/-};NgR2^{-/-};NgR3^{-/-}$ or NgR^{NNN}) show increased LTP relative to NgR controls ($NgR1^{+/-};NgR2^{+/-};NgR3^{+/-}$ or NgR^{HHH}) (Figure 2A), as revealed by the fEPSC slope average (55–60 minutes). Animals lacking other combinations of NgR alleles show no LTP alterations. These findings demonstrate all three NgRs (NgR1-3) contribute collectively to restricting LTP. No change in overall excitability of CA1 pyramidal neurons (input/output curves: Figure S2) or paired-pulse ratio (PPR) was observed in NgR^{NNN} animals, suggesting augmented LTP resulting from NgR family loss is likely due to some postsynaptic alteration.

To address whether NgRs mediate Aβ inhibition of synaptic plasticity (Walsh et al., 2002), we assessed ADDL inhibition of LTP in our hippocampal slice preparations. Consistent with previous work, we observe a decrease in LTP following ADDL exposure (150 nM) in control slices (Figure 2B). Strikingly, in NgR family knockouts (NgR^{NNN}), we find ADDL inhibition of LTP is reversed, reaching a fEPSC slope indistinguishable from NgR^{NNN} animals alone. These observations demonstrate the NgR family is required for Aβ's inhibition of synaptic plasticity.

To determine whether Aβ functions via known intracellular mediators of NgR signaling (Wills et al., 2012), we asked if Rho Kinase (ROCK) is required for Aβ's inhibition of LTP. We find preincubation of brain slices with a ROCK inhibitor, Y27632 (1μM), reverses ADDL's inhibition of LTP (Figure 2C), similar to NgR family loss. Interestingly, in control neurons we find ROCK inhibition (Y27632) blocks LTP (Figure 2C), in contrast to NgR family loss. These observations are consistent with previous work demonstrating ROCK is required for LTP (Rex et al., 2009). These findings suggest NgRs and ROCK have distinct roles in regulating LTP under physiological conditions but under pathological conditions modeling AD, the NgR-ROCK signaling pathway is recruited to mediate Aβ's synaptic pathologies.

Consistent with these findings, we observe ROCK inhibition (Y27632; 1μM) reverses LTP deficits in an AD mouse model (*3xTG-AD*; Oddo et al, 2003), where patient mutations have been engineered in presenilin, APP and tau (Figure 2D). Overall excitability (input/output curves; Figure S2) and PPR is unaltered in *3xTG-AD* mice, suggesting LTP deficit in these animals has a postsynaptic origin.

ADDLs bind NgR1 on the Dendritic Shaft of Neurons

Given our findings that NgRs mediate numerous effects of Aβ, we considered whether NgRs might be receptors for ADDLs. Previous work demonstrated that NgR1 binds monomeric Aβ 1-42 peptide (Park et al., 2006). However, NgR1 binding to oligomeric Aβ (ADDLs) has not been examined, nor has NgR2 or NgR3's affinity for ADDLs been investigated. To address these questions, biotin-tagged Aβ 1-42 peptide oligomers (ADDLs) were prepared as described earlier (Figure S1). The concentration and size of biotin-tagged ADDLs and monomeric Aβ 1-42 (ABm) was confirmed by HPLC, SEC and EM.

When NgR family members are expressed in heterologous cells, we find biotin-tagged ADDLs bind NgR1 (Figure 3A–C), but not NgR2 or NgR3. These observations suggest among NgR family members only NgR1 binds ADDLs. A quantification of the size and intensity of Aβ puncta demonstrates ADDLs bind more avidly to NgR1 than monomeric Aβ (ABm).

To assess whether NgR1 functions as an Aβ receptor during synapse development, ADDL binding studies were carried out on primary hippocampal neuron cultures following the expression of an shRNAi previously validated to eliminate NgR1 cell surface expression (Wills et al., 2012). shRNAi targeting of NgR1 resulted in a markedly reduction in ADDL binding along GFP-positive dendritic shafts of neurons, both in terms of puncta density and intensity (Figure 3D–E). Further, ADDL binding was reduced at synaptic sites following NgR1 loss, highlighted by immunostaining with the postsynaptic protein PSD95. Consistent with these findings, ADDLs and NgR1 colocalize predominantly at asynaptic sites along the dendritic arbor of hippocampal neurons, as revealed by ADDL-NgR1 immunostaining (Figure 3G). These experiments suggest NgR1 mediates Aβ's inhibition of synapse assembly and plasticity by binding ADDLs at asynaptic sites along the dendritic arbor.

ADDLs Activate RhoA and Inhibit Calcium Signaling in the Dendritic Shaft

To define the initiating site of Aβ's synaptic pathologies mediated by NgR1, we developed an imaging approach to visualize Aβ-NgR signaling live in neurons. Our current work suggested RhoA is a likely mediator of Aβ-NgR signaling. We hypothesized visualizing RhoA activity in neurons following Aβ exposure would identify where Aβ-NgR signaling is initiated. To track RhoA activity, we introduced a RhoA FRET (Förester resonance energy transfer) sensor (RhoA2G; Fritz et al., 2013- Figure S3A) into hippocampal neurons. Our validation studies illustrate the RhoA2G sensor can resolve RhoA activity in hippocampal neurons cultures (Figure S3A–G). To assess sensor activity, regions of interest (ROIs: 5–10 μm boxes) were defined along the dendritic shaft, soma, spine and axon. Photoacceptor bleaching studies demonstrate the fluorescence emissions from the RhoA sensor are FRET signals, since bleaching of the photoacceptor vGFP results in a rise in the donor fluorophore mTFP (Figure S3E), a defining feature of FRET (Nakamura et al., 2005). Pharmacological modulators of RhoA ((LPA- activator) or (C3- inhibitor)) alter RhoA2G sensor activity when perfused onto neurons (Figure S3F), demonstrating we can detect acute perturbations in RhoA activity. Overexpression of a known RhoA GAP (GTPase-Activating Protein; P50 GAP) or RhoA GEF (Guanine Exchange Factor; DBL) alter baseline RhoA2G activity

relative to control neurons (Pertz et al., 2006), showing we can detect chronic changes in RhoA activity (Figure S3G).

To visualize calcium responses to ADDLs in neurons, we expressed a red-shifted genetically encoded calcium sensor ((RCaMP); Akerboom et al., 2013- Figure S3B) along with RhoA2G into neurons, since Aβ exposure increases intracellular calcium in neurons (Um et al., 2013). Glutamate uncaging studies demonstrate RCaMP can resolve small calcium changes in the dendritic spine (Figure S3H). KCl perfusion onto neurons shows RCaMP has a robust dynamic range and detects changes in calcium in axons, dendrites and spines (Figure S3I). Importantly, we can resolve RhoA2G (vGFP/mTFP) and RCaMP (mRuby) sensor emissions simultaneously using spectral imaging and unmixing (Figure S3C–D), since simultaneous (457 and 561nm) or individual (457 or 561nm) excitation of RhoA2G and RCAMP sensors results in comparable measures of fluorophore emission. Lastly, we observe no detrimental effects on cell health, dendritic growth or synapse density by coexpression of RhoA2G and RCaMP in neurons (Figure 3A and data not shown).

Following ADDL addition onto neurons expressing both RCaMP and RhoA2G sensors, we observe calcium and RhoA responses with distinct temporal and spatial characteristics. ADDLs elicit a short-lived calcium peak in both dendrites and spines (Figure 4A–C, Figure S4A). Following this acute response, we observe a long-lasting reduction in calcium (>15 minutes) that is specific to the dendritic shaft (Movie#1). Interestingly, coincident with the Aβ-induced reduction in calcium in the dendritic shaft, we observe a long-lasting rise in RhoA activity. In contrast, ADDL exposure to dendritic spines results in a modest long-term increase in both RhoA and calcium (Figure 4C, Figure S4A). ADDL exposure has no effect on calcium activity in axons but does result in a small rise in RhoA (Figure S4E). Controls including DMSO alone, Aβ 42-1 peptide and Aβ 1-42 monomer do not alter calcium or RhoA sensors (Figure S4G). ADDL exposure not only reduces baseline calcium activity in dendrites but also calcium transients associated with synaptic growth (Figure S4I; Lohmann et al., 2008). These observations suggest Aβ triggers distinct signaling events in the dendritic shaft, spines and axons of hippocampal neurons.

To address whether Aβ functions via NgR1 to modulate RhoA and calcium signaling we imaged neurons where NgR1 had been targeted by shRNAi (Wills et al., 2012). Following RNAi-mediated loss of NgR1, neurons exposed to ADDLs do not activate RhoA or inhibit calcium signaling in shaft ROIs (Figure 4D, S4C and S4H). Consistent with this finding, dendritic calcium transients are also unaffected by ADDLs in NgR-minus neurons (Figure S4I). Further, in dendritic spines lacking NgR1, ADDLs no longer trigger RhoA and calcium activity (S4H).

Naturally secreted soluble Aβ oligomers more closely resemble Aβ peptides isolated from AD patients and inhibit synaptic plasticity at lower concentrations than synthetic Aβ oligomers (Welzel et al., 2014). We isolated soluble Aβ peptides secreted from cultured cells expressing an AD associated mutant (APP^{V717F}; 7PA2 cells), confirmed their oligomeric status by western blot analysis (data not shown) and exposed neurons to soluble oligomers. In cultured hippocampal neurons expressing RhoA2G and RCaMP sensors, soluble Aβ oligomers (7PA2) activate RhoA and inhibit calcium signaling along the dendritic shaft,

analogous to synthetic ADDLs (Figure S4B). Further, neurons lacking NgR1 (shNgR1) do not activate RhoA or inhibit calcium signaling following 7PA2 cell extract exposure (Figure S4C), demonstrating soluble Aβ oligomers, like synthetic ADDLs, signal via NgR1. 7PA2 cell extracts also trigger an acute calcium rise in neurons independent of NgR1, similar to ADDLs. Note, control cell supernatant (CHO) had no effect on RhoA or calcium activity (Figure S4F). Finally, 7PA2 cell extracts reduce dendritic spine density in hippocampal slice cultures dependent on NgR1 (shNgR1- Figure S4D). These observations suggest NgR1, upon binding to Aβ oligomers, either from cell-derived or synthetic sources, triggers a sustained activation of RhoA and inhibition of calcium signaling along the dendritic shaft of hippocampal neurons that results in a reduction in dendritic spines. In contrast, acute calcium responses to Aβ in neurons is independent of NgR signaling.

NMDAR receptors mediate aspects of Aβ-dependent calcium signaling in neurons (Shankar et al., 2007; Arbel-Ornath et al., 2017). We therefore investigated the role of NMDARs in Aβ's modulation of RhoA and calcium activity in dendrites. Following NMDAR inhibition (AP5 1μM) acute calcium responses to ADDLs in the dendritic shaft of neurons are lost but long-term activation of RhoA and inhibition of calcium signaling is preserved (Figure S4E). These findings suggest Aβ acts via NMDARs to acutely increase calcium while independently signaling thru NgR to modulate RhoA and calcium activity over a longer time period.

T-Type Channels Contribute to Synapse Development, Plasticity and Calcium Signaling in Dendrites

To determine the potential calcium regulatory target of NgR-Aβ signaling in the dendritic shaft, we exposed neurons expressing RCaMP with various pharmacological blockers. Numerous voltage-gated calcium channels (VGCCs) are highly expressed in the dendritic shaft (Yasuda et al., 2003; McKay et al., 2006). We examined whether blockers of VGCCs alter RCaMP sensor levels in dendrites. Among pharmacological blockers of VGCCs, NNC and TTA-P2, inhibitors of T-type calcium channels, elicited the largest reductions in baseline calcium in dendrites (Figure 5E and S5E). None of the VGCC blockers had deleterious effect on cell health or dendritic spines over this imaging period.

T-type channels (CaV3.1, CaV3.2 and CaV3.3) are highly expressed on dendrites of hippocampal pyramidal neurons and mediate synaptic calcium signaling (McKay et al., 2006; Magee et al., 1995). Given our findings, we considered whether T-type channels contribute to synapse development. To determine T-type channel expression during synapse development, cultured hippocampal neurons were immunostained with antibodies for individual channels. Antibody specificity was confirmed by immunostaining neurons expressing shRNAis targeting individual channels (Figure S5). Antibody staining is reduced on neurons expressing shRNAis targeting each T-type channel, demonstrating the efficacy of both shRNAis and antibodies. We find CaV3.1, CaV3.2 and CaV3.3 are expressed along the dendritic shaft of hippocampal neurons (Figure 5A). Further, some staining overlaps with the post-synaptic protein PSD95, suggesting T-type channels are present at synapses.

To address whether T-type channels contribute to synaptic development, shRNAis targeting individual channels were introduced into hippocampal slice or dissociated neuron cultures

along with vGFP. RNAi targeting of CaV3.1 or CaV3.3 reduced dendritic spine density in hippocampal slice cultures relative to an shRNAi control (Figure 5B). Consistent with these findings, RNAi targeting of CaV3.1 or CaV3.3 in dissociated hippocampal neurons reduced the density of protein markers of excitatory synapses (PSD95 and Synapsin 1) relative to controls (shCON) (Figure S5B). Importantly, these shRNAis were functionally validated (Park et al., 2010 and Figure S5B). Expression of an RNAi-resistant CaV3.3 (WTVCaV3.3 (R)) rescued synapse density deficit resulting from RNAi targeting of this channel (shCaV3.3#1), demonstrating the specificity of this RNAi for CaV3.3. A second RNAi targeting CaV3.3 (shCaV3.3#2) also reduced synapse density relative to controls in these neuron cultures, corroborating our findings that CaV3.3 is necessary for synaptic development (Figure S5B). Mini-excitatory postsynaptic current (mEPSCs) recordings in dissociated neurons lacking CaV3.1 alone or CaV3.1 and CaV3.3 in combination reveal a reduced mEPSC frequency relative to controls (Figure 5C and S5C). In contrast, shRNAi targeting of CaV3.1 and CaV3.3 has no effect on mEPSC amplitude (Figure S5D). These findings suggest CaV3.1 and CaV3.3 contribute to the establishment of functional excitatory synapses during development but not their strengthening once formed. In contrast, CaV3.2 appears not to contribute to excitatory synapse development., since neither of two shRNAis targeting CaV3.2 alter spine density or markers of excitatory synapses in our studies (data not shown). Importantly, RNAi-targeting of T-type channels (shCaV3.1-3.3) eliminates NNC and TTA-P2's inhibition of calcium signaling in dendrites (Figure S5E), demonstrating the specificity of these blockers for T-type channels.

We hypothesized if T-type channels participate in Aβ signaling they should contribute to plasticity regulated by Aβ. Consistent with this hypothesis, we find the T-type channel blocker NNC inhibits LTP in acute hippocampal slices (Figure 5C). Note, NNC shows no pathological effects on dendritic spines in hippocampal slice cultures (data not shown). In contrast, nimodipine, an L-type channel blocker, has no effect on LTP. In total, these studies identify T-type channels as mediators of dendritic calcium signaling, synapse assembly and synaptic plasticity.

To address whether intracellular mediators of Aβ-NgR signaling alter calcium in dendrites, we exposed RCaMP expressing neurons to the ROCK inhibitor Y27632 (Figure 5D). Interestingly, we observe a marked rise in RCaMP activity in the dendritic shaft of neurons following ROCK inhibition, suggesting ROCK functions to restrict calcium signaling in the shaft. Note, Y27632 has no deleterious effects on neuron health (Wills et al., 2012).

ADDLs Inhibit T-Type Channels Mediating LTP Loss

Given previous work demonstrates RhoA signaling can inhibit T-type channels (Iftinca et al., 2007), we considered whether Aβ-NgR signaling inhibits synapse assembly and plasticity by blocking T-type channels. To address this question we recorded whole-cell T-type currents from cultured hippocampal neurons before and after ADDL exposure. T-type currents were isolated by a stepwise voltage regime (Figure S6 and 6A). Following ADDL exposure, we observe a marked reduction in peak amplitudes of T-type currents (Figure 6A and C). Further, ADDL exposure results in a leftward shift in activation and inactivation curves of T-type currents (G/G_{max} and I/I_{max}), suggesting Aβ alters activation and

inactivation properties of T-type channels (Figure S6B and C). ADDL's inhibition of T-type currents was comparable to T-type channel blockers NNC and TTA-P2 (Figure 6B and C). Importantly only low-voltage activated (LVA) currents are inhibited by ADDLs, not high-voltage activated (HVA) currents. Further recordings under control conditions reveal no current rundown over the recording period (Figure 6B). Finally, blocking all high voltage activated calcium channels (Agatoxin, Conotoxin and Nimodipine) had no effect on ADDL's inhibition of LVA currents (Figure S6D), suggesting among VGCCs ADDL's exclusively inhibit T-type channels.

To determine which T-type channel(s) Aβ signaling inhibits, we introduced shRNAis targeting T-type channel into neurons and exposed neurons to ADDLs. Given CaV3.1 and CaV3.3 contribute to synapse development, we combined shRNAis targeting these channels. An shRNAi targeting CaV3.2 (shCaV3.2) served as a control, since CaV3.2 does not contribute to synapse development. We find ADDLs no longer block T-type currents in neurons lacking CaV3.1 and CaV3.3, demonstrating these channels are a target of ADDL-mediated inhibition (Figure 6C). In contrast, T-type currents in shCaV3.2 expressing neurons were inhibited comparably to controls, demonstrating CaV3.2 is not a target of Aβ signaling. Recordings from shCaV3.1, shCaV3.3 expressing neurons also reveal a significant reduction in baseline currents (Figure S6C). In contrast, baseline currents in neurons expressing shCaV3.2 are unaltered. These findings demonstrate CaV3.1 and CaV3.3 channels contribute to endogenous T-type currents in hippocampal neurons during synaptic development, while CaV3.2 has no role. We hypothesize that residual current in neurons lacking CaV3.1 and CaV3.3 are from high-voltage calcium channels (Figure 6B and S6D). Finally, neither NNC or TTAP2 inhibit LV currents in neurons lacking all T-type channels (shCaV3.1-3.3), demonstrating the fidelity of our recordings and specificity of these blockers (Figure S6F).

To determine whether T-Type channels contribute to ADDL's synaptic pathologies, we examined whether blocking T-type channels (NNC) in combination with ADDL's alter the inhibition of LTP we observed with either treatment alone. We find combining NNC and ADDL has no greater inhibition of LTP than either ADDL or NNC alone (Figure 6D), consistent with Aβ inhibiting T-type channels to block synaptic plasticity.

To determine whether ADDL inhibition of T-type channels blocks calcium signaling in neurons, sensor expressing neurons lacking CaV3.1 and CaV3.3 (shCaV3.1-shCaV3.3) were exposed to ADDLs (Figure 6E). In neurons lacking CaV3.1and CaV3.3 ADDL exposure still elicits an acute peak in calcium activity and long-term activation of RhoA, but the sustained inhibition of calcium activity observed in dendrites of control neurons is lost. Acute calcium responses to ADDLs are also preserved in the dendritic spines of neurons lacking CaV3.1 and CaV3.3 (Figure S6E), while long-term activation of RCaMP and RhoA normally seen in control neurons is lost, suggesting T-type channels also contribute to Aβ signaling in spines. Neurons expressing shCaV3.2 show comparable RhoA and calcium responses to ADDLs as controls (Figure S6F). These observations suggest Aβ signaling inhibits CaV3.1 and CaV3.3 in the dendritic shaft, compromising calcium influx through these channels.

NgR Signaling Mediates ADDL Inhibition of T-Type Channels, Calcium Signaling and LTP Loss

To address whether Aβ inhibits T-type channels via NgR-Rho signaling, we asked if activating RhoA in neurons is sufficient to inhibit T-type channels. We find LPA (lysophosphatidic acid), a receptor agonist that activates RhoA (Wills et al., 2012; Figure S4F), inhibits T-type currents with a magnitude comparable to that of ADDLs (Figure 7A and C). In contrast, ROCK inhibition (Y27632 1μM) reverses ADDL's block of T-type channel currents (Figure 7B), demonstrating Aβ signaling acts via ROCK to inhibit T-type channels. RNAi-mediated knockdown of NgR1 also reverses ADDL's inhibition of T-type currents (Figure 7C), demonstrating NgR1 is the Aβ receptor activating ROCK signaling.

To determine whether ROCK mediates Aβ's inhibition of dendritic calcium signaling, we incubated sensor-expressing neurons with the ROCK inhibitor Y27632 and exposed these neurons to ADDLs (Figure 7D). Following ROCK inhibition, ADDL-mediated inhibition of dendritic calcium signaling in neurons is lost. However, following a washout of Y27632, ADDL's inhibition of dendritic calcium signaling is restored. Complimentary non-washout sensor imaging studies confirm ADDL inhibition of dendritic calcium signaling is lost following ROCK inhibition (Figure S7A). These studies demonstrate ROCK activity mediates Aβ's inhibition of T-type channel calcium influx in the dendritic shaft of neurons.

To determine if T-type channels contribute to Aβ-NgR mediated inhibition of LTP, we assessed Aβ's inhibition of LTP following ROCK inhibition (Y27632) or loss of the NgR family (NgR^{NNN}) in acute hippocampal slices. We find the T-type channel blocker NNC reverses the capacity of ROCK inhibition (Y27632) or NgR loss (NgR^{NNN}) to rescue neurons from ADDL-mediated LTP reduction (Figure 7E). These findings suggest both NgRs and ROCK function via T-type channels to mediate Aβ's LTP inhibitions. Interestingly, NNC alone reverses the augmented LTP in NgR family knockouts (NgR^{NNN}), suggesting T-type channels are also required for NgR's inhibition of LTP under normal physiological conditions.

ADDL Inhibits T-Type Channels by ROCK Phosphorylation of CaV3.1

Our work demonstrates ROCK activity is required for Aβ-mediated inhibition of T-type currents, suggesting ROCK might directly phosphorylate T-type channels. Previous work (Iftinca et al., 2007) revealed ROCK phosphorylates CaV3.1 at two consensus phosphorylation sites (M1 and M2). To determine whether Aβ inhibits T-type channels via ROCK-mediated phosphorylation of CaV3.1, we overexpressed in neurons a $CaV3.1^{M1+M2}$ mutant incapable of being phosphorylated by ROCK (Iftinca et al., 2007). Relative to WTCaV3.1, we observe a marked rescue of Aβ's inhibition of T-type currents in neurons expressing $CaV3.1^{M1+M2}$ (Figure 7F), despite comparable expression of these two CaV3.1 constructs (Figure S7B). These observations suggest the $CaV3.1^{M1+M2}$ mutant is at least partly resistant to Aβ signaling mediated inhibition, consistent with Aβ triggering ROCK phosphorylation of CaV3.1 at M1 and M2 sites. We hypothesize residual T-type currents inhibited by Aβ in neurons expressing $CaV3.1^{M1+M2}$ are from endogenously expressed T-type channels. Consistent with this hypothesis, overexpression of $CaV3.1^{M1+M2}$ did not

significantly increase baseline T-type current amplitude relative to control neurons (Figure 7SC).

To address the significance of ROCK phosphorylation of CaV3.1 in Aβ-mediated synaptic pathologies, hippocampal slice cultures overexpressing CaV3.1^{M1+M2} were exposed to ADDLs and dendritic spines analyzed. We find CaV3.1^{M1+M2} overexpression protects CA1 pyramidal neurons from ADDL-mediated reductions in spine number (Figure 7G). Interestingly, expressing the CaV3.1^{M1+M2} mutant alone in neurons increases spine density relative to controls, suggesting ROCK phosphorylation of CaV3.1 also restricts synapse assembly during development.

To address whether ROCK phosphorylation of CaV3.1 mediates ADDL's inhibition of calcium signaling in dendrites, CaV3.1^{M1+M2} along with RhoA and RCaMP sensors were coexpressed in neurons that were exposed to ADDLs (Figure S7D). In contrast to control neurons (CaV3.1^{WT}), ADDLs do not inhibit calcium signaling in CaV3.1^{M1+M2} mutant neurons. These observations suggest ROCK phosphorylation of CaV3.1 is essential for Aβ's inhibition of calcium signaling in dendrites.

ADDLs Block Learning via NgR-mediated Inhibition of Spine Assembly and T-type Channels

An important measure of Aβ pathology is its impact on learning. To determine the role of NgRs in Aβ-mediated inhibition of learning, we introduced ADDLs (~10 pmols) via a single intracerebroventricular (ICV) injection into the mouse brain (Figure 8A and S8A) and examined its impact on novel object recognition (NOR) learning. Consistent with previous work (Figueiredo et al, 2013) ADDLs block NOR learning 7 days after ICV injection in comparison to control (DMSO) injected animals (Figure 8B). In contrast, NgR family knockouts (*NgR*^{NNN}) are unaffected by ADDLs, showing normal NOR behavior (right panel). Note, none of the ICV injected animals show deficits in movement (open field analysis; Figure S8C). These findings suggest NgRs mediate Aβ's inhibition of learning.

To address whether excitatory synapse loss correlates with Aβ-dependent learning deficits, we examined dendritic spines in ADDL-injected animals expressing GFP in pyramidal neurons in the hippocampus (*Thy1-GFPm*; Feng et al., 2000). Eight days post-injection we find a significant reduction in mature dendritic spines on CA1 pyramidal neurons in ADDL-injected animals relative to controls (Figure 8C and S8D). Strikingly, ADDL injections have no effect on spines in animals lacking the NgR family (*NgR*^{NNN}), demonstrating NgRs mediate Aβ's spine deficits *in vivo*.

To determine whether NgR-mediated inhibition of T-type channels is associated with Aβ learning deficits, we examined T-type channel currents in ADDL-injected animals. Note, the T-type channel blocker NNC inhibits LV currents in our acute hippocampal slice recording, demonstrating the fidelity of our recordings (Figure S8E). Recordings from ADDL injected animals reveal a significant reduction in T-type currents relative to DMSO controls (left panel- Figure 8D and Figure S8F). In contrast, ADDL injections have no effect on T-type currents in *NgR*^{NNN} animals (right panel- Figure 8D), demonstrating NgRs are required for ADDL-mediated inhibition of T-type currents *in vivo*.

DISCUSSION

In this study we sought to visualize how neuronal exposure to Aβ oligomers (ADDLs) effects synapse assembly. While numerous studies have documented Aβ's capacity to reduce dendritic spine density, it has been largely assumed this is driven by spine elimination. We find neuron exposure to ADDLs specifically reduces new spine assembly (Figure 1A–B). Recent *in vivo* spine imaging studies of two AD mouse models reveal specific deficits in new spine assembly consistent with our work (Zou et. al., 2015). Given new spine assembly is required for learning (Hayashi-Takagi et al., 2015), we propose deficits in spine assembly following Aβ exposure may be integral to impaired learning early in AD pathology.

We sought to gain insight into how Aβ compromises new spine assembly. We identify NgR1 as a receptor mediating Aβ's inhibition of spine addition. Given new synapses are integral to learning, we examined the synaptic potentiation underlying this process, LTP (Nabavi et al., 2014). We find the NgR family (NgR1-3) restricts LTP both under physiological conditions and a pathological condition modeling AD, exposure to ADDLs. While binding studies suggest among NgR family members ADDLs only bind to NgR1, we find the NgR family is required for ADDL-mediated LTP inhibition. These findings are consistent with NgR's shared function in restricting synapse assembly during development (Wills et al., 2012). While NgR2 and NgR3 are unable to bind ADDLs, we hypothesize they recruit coreceptors or ligands requisite for mediating NgRs synaptic functions. Numerous NgR2 and NgR3 coreceptors and ligands have been implicated in AD (Mirinova and Giger, 2013) suggesting the NgR family may convey multiple signals in mediating AD pathology.

NgRs are recognized as important inhibitors of nervous system plasticity (Mirinova and Giger, 2013). We find the NgR family inhibits LTP in adulthood, expanding the catalog of its known functions. We also uncovered that amyloid beta peptides, agents believed to drive synaptic pathology in AD, act via NgRs to compromise synaptic function. Our work demonstrates that NgR1 associates with ADDLs along the dendritic shaft of neurons. Previous work implicated NgRs (NgR1-3) in AD pathology by binding APP and regulating its proteolysis (Park et al., 2006; Zhou et al., 2011). Interestingly, in the case of NgR2, binding to APP is independent of the Aβ peptide, highlighting that NgR binding to Aβ and APP may fulfill distinct functions. Administration of an NgR1 peptide was previously shown to rescue learning deficits in an AD mouse model, an effect attributed to reducing Aβ peptide production (Park et al., 2006). Our work highlights the possibility that the beneficial effects of this NgR peptide might be the result of a direct block of Aβ-NgR signaling, reversing Aβ's inhibition of new synapse assembly. What distinguishes NgRs from a growing list of Aβ receptors (Jarosz-Griffiths et al., 2016) is NgRs function under non-pathological conditions to restrict new synapse assembly, synaptic plasticity and learning, suggesting these receptors are integral to the synaptic biology gone awry in AD.

In this study we identify RhoA and Rho Kinase (ROCK) as key intracellular mediators of Aβ-NgR synaptic pathologies. Aβ signaling is known to regulate RhoA and ROCK protein stability in neurons, altering synapse number as a result (Pozueta et al., 2013). However, how Aβ-mediated RhoA activation impacted synaptogenesis was unclear. We provide evidence RhoA and ROCK are activated by Aβ-NgR signaling on dendrites to inhibit new

synapse assembly. Interestingly, under physiological conditions, ROCK is required for LTP-induced synaptic plasticity, in contrast to NgRs. This is consistent with previous work demonstrating RhoA and ROCK are required for LTP-induced spine growth (Murakoshi et al., 2011). We attribute a role for RhoA in mediating Aβ signaling in the dendritic shaft. We speculate the Aβ-RhoA mediated block in new synapse assembly on the dendritic shaft may contribute to LTP loss. LTP stimulation is known to induce new spine growth that correlates with LTP induction (Engert and Bonehoeffer, 1999); however, the functional impact of new spine growth on LTP has not been assessed. RhoA is known to activate Rho kinase, which in turn phosphorylates numerous cytoskeletal regulators (Schmandke et al., 2007). Our study reveals RhoA-ROCK signaling has an unappreciated function inhibiting calcium signaling in neurons. Sensor imaging analysis reveals ADDLs activate RhoA via NgR1 specifically in the dendritic shaft of neurons. Further, only ADDLs, not monomeric Aβ, are capable of triggering RhoA activation or altering spine density. Given monomeric Aβ binds NgR1, we presume its inability to activate RhoA in neurons is because of monomeric Aβ's reduced affinity for NgR1 or a coreceptor relative to ADDLs. Strikingly, following neuronal exposure to ADDLs, calcium signaling is specifically inhibited along the dendritic shaft, correlating with a rise in RhoA activity. In contrast, in spines ADDLs activate RhoA and calcium signaling. We speculate RhoA signaling may target distinct calcium regulatory substrates in dendrites, spines and axons.

Calcium dysregulation is a hallmark feature of pathology in AD and models of the disease (Bezprozvanny and Mattson, 2008). Numerous calcium modulators have been implicated in AD pathology, but a clear understanding of how calcium dysregulation in is initiated in the disease is lacking. We sought to track the initiating events driving calcium dysregulation and define its cellular mediators. We find Aβ exposure drives an acute rise in calcium that is initiated in spines and dependent on NMDARs. These observations are consistent with *in vivo* studies demonstrating ADDLs trigger calcium overload in neurons dependent on NMDARs (Arbel-Ornath et al., 2017). Over a period of days, NMDAR-dependent calcium influx is reduced following neuronal exposure to ADDLs, leading to synaptic depression (Shankar et al., 2007). Our study illustrates there are alterations in calcium signaling independent of NMDARs, occurring over an intermediate period and resulting in reduced levels of calcium specifically in the dendritic shaft of neurons. Interestingly, this loss of calcium in the shaft is coincident with a rise in RhoA activity and is depends on NgR1, suggesting this signaling initiates Aβ-NgR synaptic biology. Given new spines form along the dendritic shaft, we propose Aβ-NgR mediated inhibition of calcium signaling compromises new synapse assembly.

T-type calcium channels are important calcium regulators in the dendritic shaft of pyramidal neurons in the hippocampus (Mckay et al., 2006). T-type channels expression is down regulated in the brain during aging and AD (Rice et al., 2014), suggesting reduced function of these channels may be key in driving calcium dysfunction in AD. Further, chronic inhibition of T-type channels increases Aβ peptide levels, suggesting T-type channel activity is linked with Aβ production. Our work reveals that T-type channels are a target of Aβ-NgR signaling, regulating Aβ's inhibition of spine development, synaptic plasticity and learning. Electrophysiological recordings of T-type currents demonstrate that Aβ signals via NgR and ROCK to inhibit CaV3.1 and CaV3.3. This inhibition is mediated via ROCK

phosphorylation of consensus sites on these channels that, when mutated, render it insensitive to Aβ inhibition. Further, neurons expressing this $CaV3.1^{M1,M2}$ mutant are resistant to Aβ-mediated inhibition of synapse development and the dendritic calcium loss that we propose drives pathology. The therapeutic potential of targeting T-type channels is highlighted by the identification of a drug, STK101 (ZSET1446), which enhances LTP (Moriguchi et al., 20012), reverses learning deficits in an AD mouse model (Yamaguchi et al., 2006) and is a T-type channel agonist (Yamamoto et al, 2013). STK101 has shown promising results in numerous clinical trials aimed at treating AD (Gauthier et al., 2015).

This study illustrates the importance of tracking initiating events driving synaptic pathology in AD. Our live imaging studies reveal Aβ specifically compromises new spine assembly. Sensor imaging demonstrates Aβ signaling on the dendritic shaft drives this pathology. Electrophysiology pinpoints T-type channels as the target of Aβ signaling. Finally, animal behavior studies demonstrate the relevance of NgR signaling in Aβ-mediated learning deficits. Given the array of pathologies associated with Aβ, use of such imaging-based approaches may have broader application in defining different phases of the disease state.

STAR METHODS

CONTACT FOR REAGENT AND RESOURCE SHARING

- Further information and requests for resources and reagents should be directed to and will be fulfilled by the Lead Contact, Zachary Wills (zpwills@pitt.edu).
- Requests for $NgR1^{-/-};NgR2^{-/-};NgR3^{-/-}$ mice require letters of permission from the MMRC (*NgR1; Rtn4r*^{tm1Matl}) and Lexicon Genetics (*NgR2; Rtn4rl2*^{tm1Lex} and *NgR3; Rtn4rl1*$^{Gt(OST188035)Lex}$) since NgR^{NNN} animals were generated by breeding of these animals.

EXPERIMENTAL MODEL AND SUBJECT DETAILS

Sex and Age/Developmental Stage of Experimental Models

- In LTP studies 6–10 month old animals of both sexes were used in all analyses. In *in vivo* studies following ICV injections of Abeta peptides, including Novel Object Recognition (NOR), analysis of dendritic spines and acute slice recordings of T-type currents only male mice from 8–12 weeks of age were used, since initial NOR studies in *WT* female mice (data not shown) revealed deficits in performance relative to male litter mates. Note, previous NOR studies following ICV injections of Abeta peptides also exclusively analyzed male mice (Figueiredo et al., 2013).
- *In vitro* studies of dendritic spines (live and fixed imaging) were carried out in cultured hippocampal slices isolated from P6 Long-Evans rat pups of either sex at the indicated days in cultures.
- *In vitro* studies of sensors, mEPSCs, IHC staining for synaptic proteins and T-type channel recordings were carried in dissociated neurons cultures from hippocampi dissected from E18 rat embryos of undefined sex from 3–5 month old Long-Evans pregnant females.

Species/strain of experimental models

- *NgR1*$^{-/-}$; *NgR2*$^{-/-}$; *NgR3*$^{-/-}$ (*NgR*^{NNN}) mice were described previously (Wills et al., 2012). The *NgR1*$^{-/-}$ mice were provided by Marc Tessier-Lavigne (Zheng et al., 2005). The *NgR2*$^{-/-}$ and *NgR3*$^{-/-}$ mice were obtained from Lexicon Genetics. *NgR* animals were generated by breeding *NgR*^{NNN} and *NgR*^{HHH} mice. The *Thy1-GFPm* line (Feng et al., 2001) was breed with all *NgR* animals and the *NgR* colony is maintained on a mixed background. Animals were genotyped using a PCR-based strategy (Wills et al., 2012). Primers are available upon request. All knockout strains were validated by western blot and/or RT-PCR (Wills et al., 2012). *3xTG-AD* mice (Oddo et al., 2003) were acquired from Jackson labs and genotyped based on a PCR approach suggested by the vendor. Long-Evans female rats (either pregnant or with newborn litters) were purchased from Charles River and housed prior to use. The use of these animals was approved by the Institutional Animal Care and Use Committee (IACUC) at University of Pittsburgh.
- **Husbandry and Housing Conditions:** Mice were ear-tagged and genotyped by tail snipping at P15, weened at P25 and housed in cages with littermates of the same sex under conditions approved by IACUC. Bully mice or males previously exposed to females were housed in isolation, consistent with IACUC standards. During NOR analysis, ICV injected animals in their home cage were acclimated to a new room prior to Open Field studies and NOR analysis.

METHODS DETAILS

Biochemical Preparation and Analysis of Aβ peptides—Recombinant (Aβ 1-42 Human, Ultra-Pure, HFIP) and synthetic (Biotin-LC-Aβ 1-42 Human) Abeta peptides prepared as outline in Figure S1 were analyzed by HPLC and SEC. For size exclusion chromatography analysis, 50 ml of 100mM preps of peptide were injected onto a Superdex75 5/150 GL (GE) size exclusion column on an Agilent 1200 isocratic HPLC system with a flow rate of 0.25 mL/min. Aβ peptides were momomerized by incubation in 6M guanidinium chloride. Sample retention volume was measured at 215nm and the relative retention size was compared to standards of known molecular weight. Aβ peptide concentration was determined by reverse phase HPLC chromatography. For EM, 5 μl aliquots of different Aβ samples were placed on fresh glow discharged carbon-coated grids (Electron Microscopy Sciences, Hatfield), adsorbed for 2 minutes and the excess liquid removed. Following a wash with MilliQ water, the sample was stained with uranyl acetate (1% W/V) for 45 seconds, and washed again. Samples were imaged using a Tecnai T12 microscope (FEI Company, Hillsboro, OR) operating at 120kV at a magnification of 30,000x. Images were acquired with an Ultrascan 1000 CCD camera with a post-column magnification of 1.4x. Soluble Aβ peptides were isolated from Chinese hamster ovary cells (CHO) stably expressing APP751 with the Val717Phe familial Alzheimer's disease mutation (7PA2 cells: Podlisny et al., 1995). Conditioned media from confluent 7PA2 cells or CHO control cells cultured in plain DMEM for 16hrs was concentrated ~10X (Welzel et al., 2014; YM-3 Amicon filters) before being used on neurons.

For live imaging studies in slice culture synthetic Aβ peptides were used at a concentration of 500 nM (monomer equivalent) and 7PA2 extracts used at 1–2 ~nM (Welzel et al., 2014). To study the short-term (~30 minutes) effects of Aβ peptides in sensor imaging studies, Aβ peptides were used at a concentration of 1 μM. Based on our SEC analysis and previous work (Nicoll et al., 2013; Laurén et al., 2009) we estimate the concentration of ADDLs used in this study are significantly less than one half the monomer equivalent (150 nM).

Hippocampal Slice Culture Preparation—Hippocampal slices were prepared from P5–7 Long-Evans rat pups as previously described (Wills et al., 2012). Slices were cultured under sterile conditions on nylon inserts (0.4 μm pore size, Millicell) in 6-well dishes containing 0.75ml of antibiotic-free media (MEM) supplemented with 20% horse serum. Slice cultures were transfected using a Helios Gene Gun (Biorad) at 4 DIV. For live imaging studies cultures were supplemented with Fungizone (0.25 μg/mL) and penicillin/ streptomycin (1 U/mL and 1 mg/mL, respectively).

Primary Neuron and Heterologous Cell Cultures—Hippocampal neurons were dissected from E18 Long-Evans rat embryos as previously described (Wills et al., 2012). Dissociated hippocamapl neurons (1×10^5 cells per well) were plated on acid washed 12mm coverslips coated overnight with poly-D-lysine (HMW 20 μg/ml) and Laminin (3.4 μg/ml). Neurons were cultured in Neurobasal media (Invitrogen) supplimented with 2% B27 (Invitrogen), penicillin and streptomycin (100 U/mL and 100 mg/mL, respectively), and 2 mM glutamine. Two fifths of the media was replaced in each well every 4 days. At 9 DIV, neurons were transfected using the Lipofection method (Invitrogen: Lipofectamine 2000). Neurons were trasfected with a total of 1 μg/well of DNA, including 250 ng CMV-vGFP, other plasmids of interest and PCS2 filler DNA.

HEK293T cells were plated (1×10^4 cells per well) on acid washed 12mm coverslips coated overnight with poly-D-lysine (HMW 20 μg/ml) cultured for 2hrs in DMEM supplimented with 10% fetal bovine serum, penicillin and streptomycin (100 U/mL and 100 mg/mL, respectively), and 2 mM glutamine and transfected using the Lipofection method (Invitrogen). A pDisplay NgR plasmid (750 ng) or PCS2 control DNA (750ngs) was trasfected along with cmv-vGFP (250ng) and cells were analyzed for Abeta binding 40hrs later as outlined earlier.

Chinese hamster ovary (CHO) cells expressing APP751 with the Val717Phe familial Alzheimer's disease mutation (7PA2 cells: Podlisny et al., 1995) or controls were grown in 10 cm plates in Dulbecco's modified Eagle's medium (DMEM) containing 10% fetal bovine serum, 100 units/mL penicillin, 100 μg/mL streptomycin, 2 mM L-glutamine and, in the case of 7PA2 cells, G418 (200 μg/mL) to select for cells expressing APP751. Cells were allowed to reach ~ 90% confluence before being washed and cultured in unsupplemented DMEM for 16 hrs before isolating soluble Aβ peptides.

Aβ Peptides Binding Studies—For Aβ staining studies Biotin-LC-Aβ (1-42) was added to heterolous cells tranfected with NgR receptors or 14DIV hippocamapal neurons, cultured for 1 hr at 37°C, washed and fixed as above. For Aβ-NgR1 colocalization Biotin-LC-Aβ (1-42) and an anti-NgR1 antibody ((1ug/ml) goat; R&D systems) were coincubated

with 14DIV hippocamapal neurons, cultured for 1 hr at 37°C, washed and fixed as above. A streptavidin-conjugated Alexa-555 secondary antibody (1:400; Invitrogen) was used to detect Biotin-LC-Aβ while an anti-Rat Alexa-674 antibody was used to detect the NgR1 antibody.

Immunohistochemistry and Immunocytochemistry—Antibodies were diluted in a GDB buffer (0.1% gelatin; 0.3%TX-100; 15mM Phosphate Buffer (pH 7.4); 250mM NaCl). Alexa 488, 555 and 647 (1:400 [Invitrogen]) secondary antibodies were used to visualize primary antibodies.

For immunocytochemistry, primary neurons cultured on coverslips were fixed for 8 minutes in a freshly prepared paraformaldehyde (4%) sucrose (4%) PBS (pH7.4) solution, washed and incubated with the indicated antibodies overnight at 4°C, and stained with secondary antibodies at RT for 2hrs. Coverslips were mounted on glass slides using Fluormount-G (Southern Biotech) and imaged using a Nikon A1R laser scanning confocal.

Fixation of slice cultures was performed directly on the nylon culture membrane at 11DIV in 2.5% paraformaldehyde and 4% sucrose and processed for immunohistochemistry directly on mesh cutouts. Slices were 1st incubated in a blocking buffer overnight (10% Goat Serum, 0.25% triton-X100 in PBS (pH 7.4)), immunostained with anti-GFP (1:800; Aves lab, Inc.).

For *in vivo* analysis of dendritic spines *NgR* animals coexpressing *Thy1-GFPm* (Feng et al., 2000) were perfused transcardially with fresh 4% paraformaldehyde in PBS (pH 7.4), brains were dissected out, post-fixed for 1 hour and washed overnight in PBS before vibratome sectioning (100 μm). Sections in net wells were immunostained with an anti-GFP antibody (1:800; Aves lab, Inc.) and processed identically as slices cultures above.

Spine and Sensor Imaging—As previously described (Wills et al., 2012), for live imaging studies of spine assembly hippocampal slices on mesh inserts were transferred to 35 mm dishes filled with a HEPES-based ACSF. CA1 Positions and imaging locales of GFP-positive pyramidal neurons were carefully documented and regions of interest (secondary apical dendrites) were imaged using a 60x water-dipping objective (NA 1.0). Spines were designated based on previously defined criteria (Harris et al., 1992), encompassing thin, stubby and mushroom spines (0.5 μm ≤ (spine length) L ≤ 2.5 μm; (spine width) $W_h \geq 0.5$ μm). All samples were blinded before imaging and only unblinded after dendritic spine analysis was complete.

For analysis of dendritic spines, fixed and immunostained vibratome sections from ICV injected animals were blinded for genotype and condition, then secondary proximal apical regions of CA1 pyramidal neurons from the left hippocampus (side proximal to ICV injections) were imaged by confocal microscopy (Nikon A1R at 2x zoom) using a 60x oil objective (NA 1.4). Z stacks (0.3 – 0.5 μm) were used to encompass as much of the dendritic arbor as possible. Images were subsequently deconvolved to get rid of out of focus light (Nikon Elements, Inc) and analyzed to define spine types and features (length, width and volume) using Imaris software (Bitplane).

For analysis of Biotin-LC-Aβ staining of heterologous cells transfected with NgR receptors or 14DIV hippocampal neurons, fixed and stained cells/neurons were imaged using a Nikon A1R confocal microscope. Transfected heterologous cells (GFP^+ and NgR^+) or neurons (GFP^+) were imaged at 60x in z stacks of 0.5μm slices (4–6 per cell/neuron). Maximal intensity projections (MIPs) were rendered for each image, the boundaries of cells/neurons of interest (GFP^+) were drawn in Nikon Elements, and the area ratio of Biotin-LC-Aβ staining in these ROIs (Abeta puncta size) or the intensity of this staining was calculated. All samples were blinded before imaging and only unblinded after staining analysis was complete.

For sensor imaging studies dissociated hippocampal neurons were transfected with RCaMP and RhoA sensors at 9DIV and imaged at 14-18DIV. RCaMP and RhoA (mTFP and vGFP) sensors were spectrally characterized in isolation (Nikon Inst.) and spectral unmixing (NIS Elements) was used subsequently to isolate RhoA and RCaMP emissions. Dissociated hippocampal neurons were placed in a mASCF and mature pyramidal neurons expressing moderate levels of both sensors were chosen for imaging. Neurons were usually imaged at 2Hz using a 60x water-dipping objective (NA 1.0) focused on proximal apical dendritic regions at zoom 2 (0.22 μm/pixel). RCaMP was excited with 561 nm light (0.35-0.5% power from a 20mW solid state laser) and mTFP with 457 nm light (10–25% laser power from a 40mW argon gas laser (note only 16mw at 457nm). The pinhole was opened slightly (1.6 airy units) to capture a broader signal and reduce sensor alterations resulting from focal changes (Lohmann et al., 2008). In most cases, either before or after imaging, z stack renderings (0.5 μms/slice) of the entire neuron was carried out to help in the identification of dendrites, spines and axons.

Drugs or Aβ peptides were added either by hand (pipetteman) or via a perfusion system. Glutamate uncaging was carried out in neurons cultured in Mg-free mASCF with 2mM MNI-caged Glutamate (Tocris). Focal uncaging was achieved using point stimulation with 405 nm light (10% laser power from 100mW 405 solid state laser). In most experiments, RhoA (LPA) or RCaMP (KCl) activators were added to the neurons being imaged to demonstrate sensor responsiveness.

All images were low-pass filtered (2 pixel detail, Nikon Inst), rendered as a 3 frame rolling average (~1.6 sec) and aligned to the first frame. Any changes in focus resulting from stage drift or unintentional bumping of the microscope were documented live and deleted from the final data. ΔF/F data was calculated by first measuring the mean of F over a control period (~1–10 minutes) and then expressing all data as ΔF/F for a given ROI. Dendritic ROIs (5–10 per image), interspersed along the dendrite at ~5–10 μm intervals, were ~5–8 μm in length spanning the full width of the dendritic arbor and not in close proximity to the soma, arbor bifurcations, or the ends of dendrites. The size and spacing of ROIs was based on studies of calcium signaling relevant for synaptic development and plasticity (Lohmann et al., 2008; Murakoshi et al., 2011). Spine ROIs (1–5 per image) were specified based on previously defined criteria for mature stubby or mushroom spines ($L > 0.5$ μm; $W_h \geq 0.5$ μm (Harris et al., 1992)). Axon ROIs (2–4 per image) were 4–6 μm in length.

For analyses of global calcium transients a program was written in MATLAB to detect calcium events (CalciumDetect). RCaMP sensor ΔF/F shaft ROI data was low pass filtered using a median fit and events that lasted at least 3.2 seconds and were at least 1 standard deviation from the mean were considered a calcium peak (Lohmann et al., 2008).

Electrophysiology—LTP studies were carried out on hippocampal slices from 6–9 month old mice as previously described (Oddo et al., 2003). Animals were anaesthetized with Isoflurane, decapitated, and brains were rapidly removed in ice-cold ACSF (125 mM NaCl, 2.5 mM KCl, 1.25 mM KH_2PO_4, 25 mM $NaHCO_3$, 1.2 mM $MgSO_4$, 2 mM $CaCl_2$, and 10 mM dextrose bubbled with 95% O2, 5% CO_2 [pH 7.4]). Coronal hippocampal slices (400 μm) were prepared using a vibratome and left to equilibrate in ACSF at room temperature before recording. Slices were continuously perfused with ACSF. Field excitatory postsynaptic potentials (fEPSCs) were recorded in the stratum radiatum from CA1 using a glass microelectrode. Synaptic responses were evoked by stimulating the Schaffer collateral pathway with a concentric bipolar stimulating electrode with 0.1 ms pulse width. LTP was induced by high-frequency stimulation (HFS) consisting of three trains of 100 Hz stimulation at 20 s intervals. Recordings were made every 30 s for 60 min after HFS. The fEPSP slope was measured offline using Axograph software and were expressed as a percentage of the average slope from the 15 min of baseline recordings. Slices were placed in an interface chamber, continuously perfused with aCSF, and oxygenated with a continuous flow of 95% O_2, 5% CO_2). Field excitatory postsynaptic potentials (fEPSPs) were recorded in the stratum radiatum of the CA1 using glass microelectrodes filled with aCSF. Synaptic responses were evoked by stimulation of the Schaffer collateral/commissural pathway with a concentric bipolar stimulating electrode with 0.1 ms pulse width. Input/output curves were generated using stimulus intensities from 0 to 500 μA in increments of 50 μA. PPF was assessed using an interstimulus interval of 50 ms. Baseline fEPSPs were evoked at 30% of the max fEPSP for 15 min prior to HFS. LTP was induced at baseline intensity using high-frequency stimulation (HFS) consisting of four trains of 100 Hz stimulation at 20 s intervals. Recordings were made every 30 s for 60 min after HFS. The maximum fEPSP slopes were measured offline using Axograph software and were expressed as a percentage of the average slope from the 15 min of baseline recordings. In some experiments, the stimulus intensity was raised so that baseline EPSP slopes matched the average baseline EPSP in the NonTg mice. LTP was measured as the 55–60 minute fEPSP slope. The researcher conducting recordings was in most cases blind to the genotype of the *NgR* animal under investigation until post analysis.

Voltage clamp recordings were carried out on acute slices (prepared as described for LTP studies above) or 14-21DIV dissociated hippocampal neurons cultured as described earlier. The extracellular recording solution contains 1 μM AP5, 10 μM CNQX, 1 μM TTX, 30 μM Saclofen, 20 μM bicuculline methiodide, 10 mM TEA-Cl, 130 mM NaCl, 5.4 mM KCl, 0.6mM $MgCl_2$, 0.6mM NaH_2PO_4, 1 mM $NaHCO_3$, 1.8 mM $CaCl_2$, 5.5 mM glucose and 10 mM HEPES adjusted to pH 7.4. The intracellular recording solution contains 120 mM tetramethylammonium, 10 mM EGTA, 10 mM Na_2HPO_4, 1mM GTP, 2mM ATP and 10 mM HEPES, adjusted to pH 7.2 with hydrofluoric acid. Currents were recorded using a Multiclamp 200B amplifier, Digidata 1320A A/D converter, and Clampex 10.3 software

(Molecular Devices, LLC, Sunnyvale, CA, USA). Series resistance and cell capacitance were compensated to the maximal possible extent. All recordings were performed at room temperature. For analyses of inhibitory effects on T-type currents (I/I Baseline), the current recording at the final minute of recording (16–30 minutes) was used. For acute slice recordings of T-type currents, only the left hippocampus (site proximal to ICV injections) was used for recording studies.

ICV Injections in Mice—Vehicle (2% DMSO) or ADDLs (0.8uls or ~10 pmol) were stereotaxically delivered to eight to twelve-week-old male mice (NgR^{WT}, NgR^{HHH} or NgR^{NNN}) under anesthesia to the lateral ventricle (coordinates: AP: −0.90 mm; ML: −1.90 mm; DV: −2.40 mm). Animals showing any signs of pathology (e.g. lethargic, ungroomed) post-injection were excluded from analysis.

Mouse Behavior Studies—In novel object recognition studies ICV injected animals were acclimated in two 20 minute sessions to an open field chamber. Open field movement and animal-object interactions (exploration) were recorded using a portable tripod mounted video camera. Open field analysis was carried during one 10-minute acclimatization session just prior to sample training out using automated software developed in MATLAB (Mathworks; Patel et al., 2014). Following habituation training, animals were exposed to two identical objects for 5 minutes (sample training). Following a two-hour retention period, animals were exposed to one familiar object and one novel object and videotaped for 5 minutes (test training). Exploration times for each object is expressed as interaction time with one object divided by the total interaction time with both objects. NOR videotaping and subsequent analysis was done by researchers blind to genotype and condition. Animals showing less that 10 seconds of interaction time with objects over the 5-minute test training session were excluded from analysis (Figueiredo et al., 2013).

QUANTIFICATION AND STATISTICS

All statistical analyses with n are indicated in figure legends and a supplemental data spreadsheet, along with exact numbers. All statistical analyses were carried out using Prism 7 (GraphPad Software, Inc.).

- In spine live imaging studies in hippocampal slice cultures, 3–4 independent experiments were carried out, with up to three imaging sessions (every two days) per locale. Approximately 10–20 locales (each locale from 1 neuron) were imaged per experiment. For analysis, locales clearly visualized at all time points were aligned, and spine density measurements were carried out using NIS Elements. n equals the number of independent experiments. Note, one P6 rat pup was used per condition for each experiment. Significance was assessed either by a paired Student's t test (CON vs ADDL) or one-way ANOVA with Bonferroni posthoc test (shNgR1 ADDL analysis).
- For analysis of dendritic spines from ICV injected animals, 10 dendritic segments from 6–10 neurons encompassing at least 100 spines per segment were imaged per animals. Spine criteria was defined based on previous work (Harris et al., 1992 [Mushroom spines= 0.75μm ≤ **L** ≤ 2.5μM; 0.4μm ≤ $\mathbf{W_h}$]; [Stubby

Spines= 0.5μm ≤ **L** < 0.75μM; 0.4μm ≤ $\mathbf{W_h}$]; [Filopodia = 0.4μm ≥ **L**; 0.4μm >$\mathbf{W_h}$]). n equals the number of animals analyzed. Significance was assessed one-way ANOVA with Dunnett's multiple comparison test.

- For analysis of Biotin-LC-Aβ staining of heterologous cells transfected with NgR receptors n equals the total number of cells analyzed over 3 independent experiments. Significance was assessed by two-way ANOVA with Dunnett's multiple comparison test.
- For sensor imaging analysis, the sensor ΔF/F of all ROIs of a particular type (shaft, spine, or axon) were averaged for each neuron. n equals the number of neurons analyzed from at least 3 independent experiments. To measure acute or sustained sensor responses following ABeta exposure, 30-second sensor averages were calculated for each ROI in SPSS (IBM). Acute responses to Aβ peptides represent the maximum 30-second mean sensor ΔF/F of ROIs of a particular type from the indicated number of neurons (n). Sustained responses to Aβ represent the maximum or minimum 1-minute mean sensor ΔF/F of ROIs of a particular type from the indicated number of neurons (n). For assessing the statistical significance of sensor data, paired analyses (Student's t test) of maximum mean sensor ΔF/F data (30-second or 1-minute sensor means) between control and Aβ exposure periods was carried out. Note, all example sensor images were maximal intensity projections of 30-second intervals where the maximum or minimum sensor changes were observed. For analysis of global calcium transients, calcium peaks were quantified before and following ADDL exposure (10–15 minutes) and significance assessed in paired Student's t tests with n equal to the number of neurons analyzed.
- In LTP studies, n equals the number of animals analyzed. A one-way analysis of variance (ANOVA) with a Tukey's (*NgR* alleles) or Dunnet's (all other analyses) posthoc test was used to assess significance for all multiple comparison analyses while an unpaired t test was in PPF analysis.
- For voltage clamp analysis of T-type current inhibition a paired t test was used to assess statistical significance comparing control baseline currents with current recordings at the final minute of recording (16–30 minutes) with the n equal to the number of neurons recorded. Note neurons were from at least 3 independent experiments.
- Average T-type current amplitudes were from recordings of cultured neurons *in vitro* or acute hippocampal slices *in vivo* studies. N equals the number of neurons recorded from *in vitro* (from at least 3 experiments) or animals (acute hippocampal slice) recorded from *in vivo*. Statistical significance was assessed by one-way ANOVA with Dunnet's multiple comparison test.
- In NOR behavioral studies, statistical significance was assessed using an unpaired Student's t test comparing the mean object exploration time with a fixed value of 50% (Figueiredo et al., 2013).

DATA AND SOFTWARE AVAILABILITY

Analysis software was developed for calcium peak detection in MATLAB (CalciumDetect). The code to run this software is provided in Github (see Key Resources Table).

Supplementary Material

Refer to Web version on PubMed Central for supplementary material.

Acknowledgments

This work was supported by the following grants: ADRC pilot grant (ADRC2013), a Competitive Medical Research grant (UPMC- CMRF2013), Whitehall Foundation grant (2013-05-70) and an R21 grant (MH107966). We thank Jaclyn Stopcynski for animal husbandry and neuronal dissection work and Ari Filip for pilot studies of ADDL binding. We are grateful for manuscript editing from Robert Sweet, Sarah Ross, Catherine Ross and Amantha Thathiah. We thank Elias Aizenman, Gerald Gebhart and Michael Gold for use of electrophysiology equipment and Simon Watkins and the Center for Biological Imaging (UPitt) for use of their microscopes and software. We thank Terry Snutch for CaV3.1 M1, M2 expression constructs and sequencing primers, Loren Looger for the RCaMPh1 expression construct and Dennis Selkoe for 7PA2 cells.

References

Arbel-Ornath M, Hudry E, Boivin JR, Hashimoto T, Takeda S, Kuchibhotla KV, et al. Soluble oligomeric amyloid-β induces calcium dyshomeostasis that precedes synapse loss in the living mouse brain. Molecular Neurodegeneration. 2017; 12:27–14. 1–14. [PubMed: 28327181]

Akerboom J, Carreras Calderon N, Tian L, Wabnig S, Prigge M, Tolo J, Gordus A, Orger MB, Severi KE, Macklin JJ, et al. Genetically encoded calcium indicators for multi-color neural activity imaging and combination with optogenetics. Front Mol Neurosci. 2013; 6:2. [PubMed: 23459413]

Bezprozvanny I, Mattson M. Neuronal calcium mishandling and the pathogenesis of Alzheimer's disease. Trends Neurosci. 2008; 31(9):454–463. [PubMed: 18675468]

Buckner R. Memory and executive function in aging and AD: multiple factors that cause decline and reserve factors that compensate. Neuron. 2004; 44(1):195–208. [PubMed: 15450170]

Busche MA, Chen X, Henning HA, Reichwald J, Staufenbiel M, Sakmann B, Konnerth A. Critical role of soluble amyloid-β for early hippocampal hyperactivity in a mouse model of Alzheimer's disease. Proc Natl Acad Sci U S A. 2012; 109(22):8740–8745. [PubMed: 22592800]

Cribbs L, Lee J, Yang J, Satin J, Zhang Y, Daud A, Barclay J, Williamson M, Fox M, Rees M, Perez-Reyes E. Cloning and characterization of alpha1H from human heart, a member of the T-type Ca2+ channel gene family. Circ Res. 1998; 83(1):103–9. [PubMed: 9670923]

Fritz RD, Letzelter M, Reimann A, Martin K, Fusco L, Ritsma L, Ponsioen B, Fluri E, et al. A versatile toolkit to produce sensitive FRET biosensors to visualize signaling in time and space. Sci Signal. 2013; 6:I.

Fu M, Yu X, Lu J, Zuo Y. Repetitive motor learning induces coordinated formation of clustered dendritic spines in vivo. Nature. 2012; 482(7387):92–95.

Gauthier S, Rountree S, Finn S, LaPlante B, Weber E, Oltersdorf T. Effects of the Acetylcholine Release Agent ST101 with Donepezil in Alzheimer's Disease: A Randomized Phase 2 Study. J Alzheimers Dis. 2015; 48(2):473–481. [PubMed: 26402011]

Gomora J, Murbartian J, Arias J, Lee J, Perez-Reyes E. Cloning and expression of the human T-type channel Ca(v)3.3: insights into prepulse facilitation. Biophys J. 2002; 83(1):229–41. [PubMed: 12080115]

Engert F, Bonhoeffer T. Dendritic spine changes associated with hippocampal long-term synaptic plasticity. Nature. 1999; 399:66–70. [PubMed: 10331391]

Feng G, Mellor RH, Bernstein M, Keller-Peck C, Nguyen QT, Wallace M, Nerbonne, et al. Imaging neuronal subsets in transgenic mice expressing multiple spectral variants of GFP. Neuron. 2000; 28:41–51. [PubMed: 11086982]

Figueiredo C, Clarke J, Ledo J, Ribeiro F, Costa C, Melo H, Mota-Sales A, Saraiva L, et al. Memantine Rescues Transient Cognitive Impairment Caused by High-Molecular-Weight Aβ Oligomers but Not the Persistent Impairment Induced by Low-Molecular-Weight Oligomers. J Neurosci. 2013; 33(23):9626–9634. [PubMed: 23739959]

Harris KM, Jensen FE, Tsao B. Three-dimensional structure of dendritic spines and synapses in rat hippocampus (CA1) at postnatal day 15 and adult ages: implications for the maturation of synaptic physiology and long-term potentiation. J Neurosci. 1992; 12(7):2685–2705. [PubMed: 1613552]

Hayashi-Takagi A, Yagishita S, Nakamura M, Shirai F, Wu YI, Loshbaugh AL, et al. Labelling and optical erasure of synaptic memory traces in the motor cortex. Nature. 2015; 525:333–338. [PubMed: 26352471]

Iftinca M, Hamid J, Chen L, Varela D, Tadayonnejad R, Altier C, Turner RW, Zamponi GW. Regulation of T-type calcium channels by Rho-associated kinase. Nat Neurosci. 2007; 10:854–860. [PubMed: 17558400]

Jack C, Knopman DS, Jagust W, Petersen R, Weiner M, Aisen P, Shaw L, Vemuri P, et al. Personal View Tracking pathophysiological processes in Alzheimer's disease: an updated hypothetical model of dynamic biomarkers. Lancet Neurology. 2013; 12:207–216. [PubMed: 23332364]

Jarosz-Griffiths HH, Noble E, Rushworth JV, Hooper NM. Amyloid-beta Receptors: The Good, the Bad, and the Prion Protein. J Biol Chem. 2016; 291:3174–3183. [PubMed: 26719327]

Kim T, Vidal G, Djurisic M, William C, Birnbaum M, Garcia K, Hyman B, Shatz C. Human LilrB2 is a β-amyloid receptor and its murine homolog PirB regulates synaptic plasticity in an Alzheimer's model. Science. 2013; 341:1399–1404. [PubMed: 24052308]

Laurén J, Gimbel DA, Nygaard HB, Gilbert JW, Strittmatter SM. Cellular prion protein mediates impairment of synaptic plasticity by amyloid-beta oligomers. Nature. 2009; 457(7233):1128–1132. [PubMed: 19242475]

Li S, Jin M, Koeglsperger T, Shepardson N, Shankar G, Selkoe D. Soluble Aβ Oligomers Inhibit Long-Term Potentiation through a Mechanism Involving Excessive Activation of Extrasynaptic NR2B-Containing NMDA Receptors. J Neurosci. 2011; 31:6627–6638. [PubMed: 21543591]

Lohmann C, Bonhoeffer T. A role for local calcium signaling in rapid synaptic partner selection by dendritic filopodia. Neuron. 2008; 59:253–260. [PubMed: 18667153]

Magee JC, Christofi G, Miyakawa H, Christie B, Lasser-Ross N, Johnston D. Subthreshold synaptic activation of voltage-gated Ca2+ channels mediates a localized Ca2+ influx into the dendrites of hippocampal pyramidal neurons. J Neurophys. 1995; 74:1335–1342.

McKay BE, McRory JE, Molineux ML, Hamid J, Snutch TP, Zamponi GW, Turner RW. Ca(V)3 T-type calcium channel isoforms differentially distribute to somatic and dendritic compartments in rat central neurons. The European Journal of Neuroscience. 2006; 24(9):2581–2594. [PubMed: 17100846]

Mironova YA, Giger RJ. Where no synapses go: gatekeepers of circuit remodeling and synaptic strength. Trends Neurosci. 2013; 36:363–373. [PubMed: 23642707]

Moriguchi S, Shioda N, Yamamoto Y, Tagashira H, Fukunaga K. The T-type voltage-gated calcium channel as a molecular target of the novel cognitive enhancer ST101: enhancement of long-term potentiation and CaMKII autophosphorylation in rat cortical slices. J Neurochem. 2012; 121:44–53. [PubMed: 22251222]

Murakoshi H, Wang H, Yasuda R. Local, persistent activation of Rho GTPases during plasticity of single dendritic spines. Nature. 2011; 472:100–104. [PubMed: 21423166]

Nabavi S, Fox R, Proulx C, Lin J, Tsien R, Malinow R. Engineering a memory with LTD and LTP. Nature. 2014; 511:348–352. [PubMed: 24896183]

Nakamura T, Aoki K, Matsuda M. Monitoring spatio-temporal regulation of Ras and Rho GTPase with GFP-based FRET probes. Methods. 2005; 37:146–153. [PubMed: 16288890]

Nicoll AJ, Panico S, Freir DB, Wright D, Terry C, Risse E, Herron CE, O'Malley T, et al. Amyloid-beta nanotubes are associated with prion protein-dependent synaptotoxicity. Nat Commun. 2013; 4:2416. [PubMed: 24022506]

Oddo S, Caccamo A, Shepherd JD, Murphy MP, Golde TE, Kayed R, Metherate R, et al. Triple-transgenic model of Alzheimer's disease with plaques and tangles: intracellular Abeta and synaptic dysfunction. Neuron. 2003; 39:409–421. [PubMed: 12895417]

Park JH, Widi GA, Gimbel DA, Harel NY, Lee DHS, Strittmatter SM. Subcutaneous Nogo receptor removes brain amyloid-beta and improves spatial memory in Alzheimer's transgenic mice. J Neurosci. 2006b; 26:13279–13286. [PubMed: 17182778]

Park Y, Park H, Lee C, Choi S, Jo S, Choi H, Kim Y, Shin H, Llinas R, Kim D. CaV3.1 is a tremor rhythm pacemaker in the inferior olive. Proc Natl Acad Sci. 2010; 107:10731–6. [PubMed: 20498062]

Patel TP, Gullotti DM, Hernandez P, O'Brien WT, Capehart BP, Morrison B, et al. An open-source toolbox for automated phenotyping of mice in behavioral tasks. Frontiers in Behavioral Neuroscience. 2014; 8:349. [PubMed: 25339878]

Pertz O, Hodgson L, Klemke RL, Hahn KM. Spatiotemporal dynamics of RhoA activity in migrating cells. Nature. 2006; 440:1069–1072. [PubMed: 16547516]

Podlisny MB, Ostaszewski BL, Squazzo SL, Koo EH, Rydell RE, Teplow DB, Selkoe DJ. Aggregation of secreted amyloid beta-protein into sodium dodecyl sulfate-stable oligomers in cell culture. J Bio Chem. 1995; 270(16):9564–9570. [PubMed: 7721886]

Pozueta J, Lefort R, Ribe EM, Troy CM, Arancio O, Shelanski M. Caspase-2 is required for dendritic spine and behavioural alterations in J20 APP transgenic mice. Nature. 2013; 4:1–12.

Rex C, Chen L, Sharma A, Liu J, Babayan A, Gall C, Lynch G. Different Rho GTPase–dependent signaling pathways initiate sequential steps in the consolidation of long-term potentiation. J Cell Biol. 2009; 186:85–97. [PubMed: 19596849]

Rice RA, Berchtold NC, Cotman CW, Green KN. Age-related downregulation of the CaV3.1 T-type calcium channel as a mediator of amyloid beta production. Neurobiol Aging. 2014; 35:1002–1011. [PubMed: 24268883]

Rousset M, Cens T, Menard C, Bowerman M, Bellis M, Brusés J, et al. Regulation of neuronal high-voltage activated CaV2 Ca2+ channels by the small GTPase RhoA. Neuropharmacology. 2015; 97(C):201–209. [PubMed: 26044639]

Schram MT, Trompet S, Kamper AM, de Craen AJ, Hofman A, Euser SM, Breteler MM, Westendorp RG. Serum calcium and cognitive function in old age. J Am Geriatr Soc. 2007; 55:1786–1792. [PubMed: 17979900]

Schmandke A, Schmandke A, Strittmatter S. ROCK and Rho: biochemistry and neuronal functions of Rho-associated protein kinases. Neuroscientist. 2007; 13:454–469. [PubMed: 17901255]

Selkoe DJ. Alzheimer's disease: genes, proteins, and therapy. Physiol Rev. 2001; 81:741–766. [PubMed: 11274343]

Shankar GM, Bloodgood BL, Townsend M, Walsh DM, Selkoe DJ, Sabatini BL. Natural oligomers of the Alzheimer amyloid-beta protein induce reversible synapse loss by modulating an NMDA-type glutamate receptor-dependent signaling pathway. J Neurosci. 2007; 27:2866–2875. [PubMed: 17360908]

Shankar GM, Li S, Mehta TH, Garcia-Munoz A, Shepardson NE, Smith I, Brett FM, et al. Amyloid-beta protein dimers isolated directly from Alzheimer's brains impair synaptic plasticity and memory. Nat Med. 2008; 14:837–842. [PubMed: 18568035]

Tanzi RE. The synaptic Abeta hypothesis of Alzheimer disease. Nat Neurosci. 2005; 8:977–979. [PubMed: 16047022]

Um JW, Kaufman AC, Kostylev M, Heiss JK, Stagi M, Takahashi H, Kerrisk ME, et al. Metabotropic glutamate receptor 5 is a coreceptor for Alzheimer abeta oligomer bound to cellular prion protein. Neuron. 2013; 79:887–902. [PubMed: 24012003]

Walsh DM, Klyubin I, Fadeeva JV, Cullen WK, Anwyl R, Wolfe MS, Rowan MJ, Selkoe DJ. Naturally secreted oligomers of amyloid beta protein potently inhibit hippocampal long-term potentiation in vivo. Nature. 2002; 416:535–539. [PubMed: 11932745]

Welzel AT, Maggio JE, Shankar GM, Walker DE, Ostaszewski BL, Li S, et al. Secreted Amyloid β-Proteins in a Cell Culture Model Include N-Terminally Extended Peptides That Impair Synaptic Plasticity. Biochemistry. 2014; 53(24):3908–3921. [PubMed: 24840308]

Wills ZP, Mandel-Brehm C, Mardinly AR, McCord AE, Giger RJ, Greenberg ME. The nogo receptor family restricts synapse number in the developing hippocampus. Neuron. 2012; 73:466–481. [PubMed: 22325200]

Xu T, Yu X, Perlik AJ, Tobin WF, Zweig JA, Tennant K, Jones T, Zuo Y. Rapid formation and selective stabilization of synapses for enduring motor memories. Nature. 2009; 462:915–919. [PubMed: 19946267]

Yang G, Pan F, Gan WB. Stably maintained dendritic spines are associated with lifelong memories. Nature. 2009; 462:920–924. [PubMed: 19946265]

Yasuda R, Sabatini BL, Svoboda K. Plasticity of calcium channels in dendritic spines. Nat Neurosci. 2003; 6:948–955. [PubMed: 12937422]

Yamaguchi Y, Miyashita H, Tsunekawa H, Mouri A, Kim HC, Saito K, Matsuno T, et al. Effects of a novel cognitive enhancer, spiro[imidazo-[1,2-a]pyridine-3,2-indan]-2(3H)-one (ZSET1446), on learning impairments induced by amyloid-beta1-40 in the rat. J Pharmacol Exp Ther. 2006; 317:1079–1087. [PubMed: 16474004]

Yamamoto Y, Shioda N, Han F, Moriguchi S, Fukunaga K. Novel cognitive enhancer ST101 enhances acetylcholine release in mouse dorsal hippocampus through T-type voltage-gated calcium channel stimulation. J Pharmacol Sci. 2013; 121:212–226. [PubMed: 23449490]

Zemmar A, Weinmann O, Kellner Y, Yu X, Vicente R, Gullo M, Kasper H, Lussi K, Ristic Z, et al. Neutralization of Nogo-A enhances synaptic plasticity in the rodent motor cortex and improves motor learning in vivo. J Neurosci. 2014; 34:8685–8698. [PubMed: 24966370]

Zheng B, Atwal J, Ho C, Case L, He XL, Garcia KC, et al. Genetic deletion of the Nogo receptor does not reduce neurite inhibition in vitro or promote corticospinal tract regeneration in vivo. Proc Natl Acad Sci U S A. 2005; 102(4):1205–1210. [PubMed: 15647357]

Zhou X, Hu X, He W, Tang X, Shi Q, Zhang Z, Yan R. Interaction between amyloid precursor protein and Nogo receptors regulates amyloid deposition. FASEB. 2011; 25(9):3146–3156.

Zou C, Montagna E, Shi E, Peters F, Blazquez-Llorca L, Shi S, Filser S, Dorostkar M, Herms J. Intraneuronal APP and extracellular Aβ independently cause dendritic spine pathology in transgenic mouse models of Alzheimer's disease. Acta Neuropathol. 2015; 129:909–920. [PubMed: 25862638]

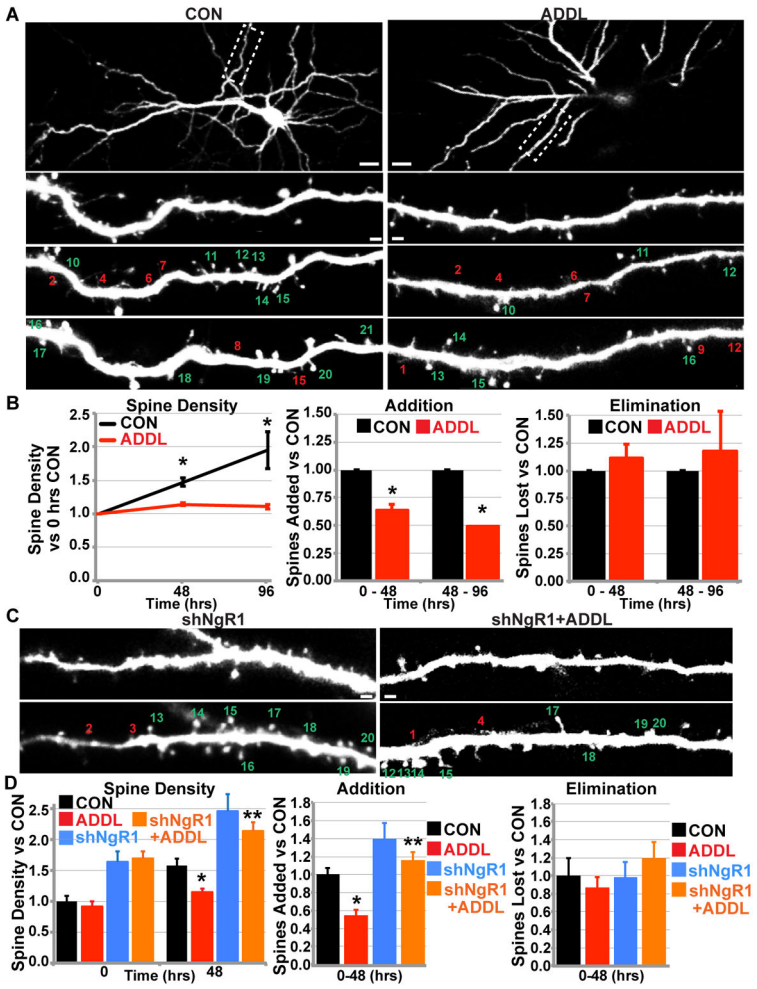

Fig. 1. ADDLs Inhibit New Spine Assembly Dependent on NgRs

(A) Live imaging of hippocampal slices reveals ADDLs (150nM) reduce dendritic spine density relative to controls (CON-0.02% DMSO) by inhibiting new spine assembly. (Top) Representative images of CA1 pyramidal neurons (9 days in vitro (DIV)) labelled with vGFP reveal (higher magnification below) a decrease in new (green<48hr old) and persistent spines (white>48hr old) following ADDL exposure but no effect on eliminated spines (lost within last 48 hr). Scale bars=10μm (top), 1μm (below).

(B) (Left) Spine density quantification reveals ADDL exposure (red) reduces spine density at indicated times relative to CON (black). Quantification of spine addition (middle) and elimination (right) reveals ADDL exposure reduces spine addition at indicated times relative to control but has no effect on spine elimination. *p<0.02 vs CON. Student's t test. n=3 experiments. Data are means, error bars represent SEM.

(C) Representative high magnification images of CA1 pyramidal neurons expressing shNgR1 and vGFP reveal at 48-hour time period NgR1 loss rescues neurons from ADDL-mediated inhibition of spine addition (green) with no effect on spine elimination (red).

(D) (Left) Quantification of mean spine density reveals ADDL-mediated reduction in spines (red) is reversed following shNgR1 expression (orange) relative to CON (black) at 48 hours. Quantification of spine addition (middle) and elimination (right) reveals NgR1 loss (orange)

reverses ADDL-mediated inhibition of spine addition (red) but has no effect on spine elimination. *p<0.05 vs CON. **p<0.0001 vs ADDL. One-way ANOVA Tukey's posthoc test. n=3 experiments. Data are means, error bars represent SEM. See also Figure S1 and Table S1.

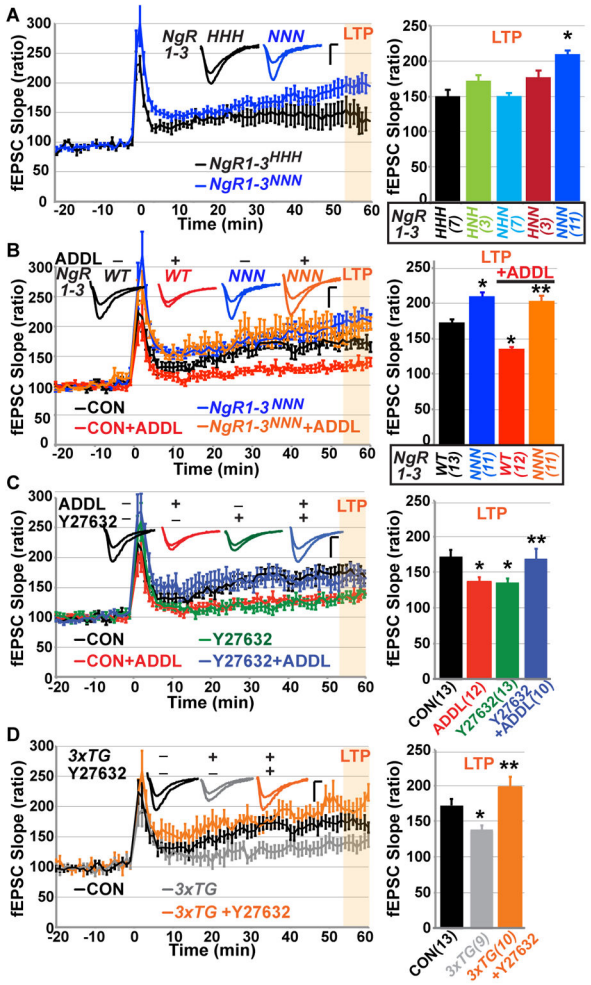

Fig. 2. NgRs and ROCK Mediate ADDL Inhibition of LTP

(A) (Left) NgR family knockouts (NgR^{NNN}) show increased LTP relative to controls (NgR^{HHH}) from fEPSC recordings at Schaffer collateral-CA1 synapses from acute hippocampal slices (6 months). Example traces above for all (calibration 0.5mV, 5ms) (Right) Mean fEPSC 55–60 min post stimulation for indicated NgR alleles. *p<0.0001 vs CON (NgR^{HHH}). One-way ANOVA Dunnett's posthoc test. n in parentheses. Data are means, error bars represent SEM.

(B) (Left) NgR family loss (NgR^{NNN}) reverses LTP deficits following hippocampal slice exposure to ADDLs (150nM). (right) 55–60 min mean fEPSC post stimulation for indicated conditions. *p<0.001 vs CON (NgR^{WT}). **p<0.0001 vs ADDL. One-way ANOVA Tukey's posthoc test. n in parentheses. Data are means, error bars represent SEM.

(C) (Left) ROCK inhibition (Y27632- 1μM) reverses LTP deficits following hippocampal slice exposure to ADDLs (150nM). (Right) 55–60 min mean fEPSC post stimulation for indicated conditions. *p<0.03 vs CON (*WT*). **p<0.05 vs ADDL. One-way ANOVA Tukey's posthoc test. n in parentheses. Data are means, error bars represent SEM.

(D) (Left) ROCK inhibition (Y27632- 1μM) reverses LTP deficits in hippocampal slice in *3xTG-AD* mice. (Right) 55–60 mean fEPSC min post stimulation for indicated conditions.

*p<0.05 vs CON (*WT*). **p<0.001 vs *3xTG-AD*. One-way ANOVA Tukey's posthoc test. n in parentheses. Data are means, error bars represent SEM. See also Figure S2 and Table S1.

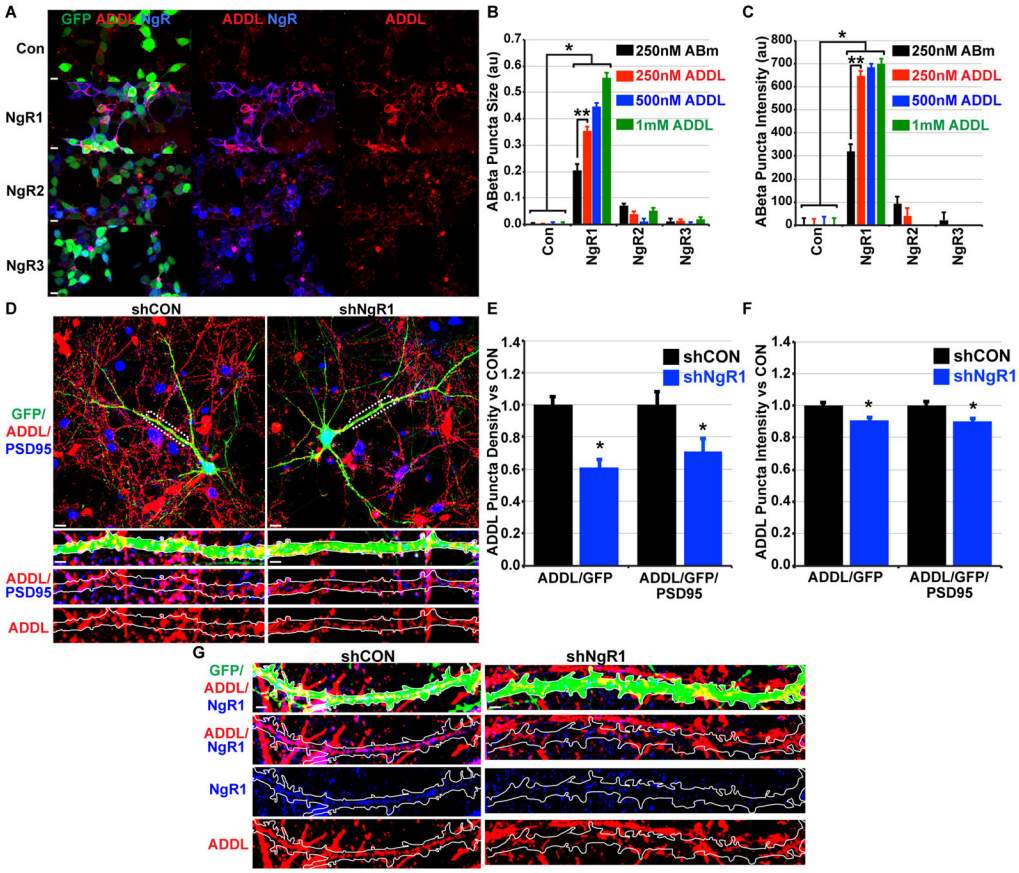

Fig. 3. ADDLs Bind NgR1 on Heterologous Cells and Neurons

(A) Heterologous cells expressing indicted NgR along with GFP (green) were live-labeled with biotin-tagged Aβ peptides, fixed and stained with anti-NgR antibodies (blue) and anti-streptavidin (red). Arrows indicate sites of ADDL-NgR1 staining. Scale bars=10 μm.

(B) Quantification of Abeta puncta size on GFP^+, NgR^+ cells following peptide incubation at indicated concentrations. *p<0.0001 vs controls (Con). **p<0.0001 vs Aβ monomer (ABm). 2-Way ANOVA Dunnett's (*) or Tukey's (**) posthoc test. n=50 cells/3 experiments. Data are means, error bars represent SEM.

(C) Quantification of Abeta puncta intensity on GFP^+, NgR^+ cells following peptide incubation at indicated concentrations. *p<0.0001 vs Con. **p<0.0001 vs ABm. 2-Way ANOVA Dunnett's (*) or Tukey's (**) posthoc test. n=50 cells/3 experiments. Data are means, error bars represent SEM.

(D) 14 DIV primary hippocampal neuron cultures expressing indicated shRNAi and GFP were live-labeled with biotin-tagged ADDLs (250nM), fixed and stained with anti-PSD95 (blue) and strepavidin (red). Boxed regions highlighted below with indicated staining. Arrowheads mark ADDL/PSD95 costaining on GFP^+ dendrites. Scale bars=10μm (top), 1μm (below).

(E) Quantification of ADDL puncta density on GFP^+ or GFP^+ $PSD95^+$ regions of neurons following peptide incubation. *p<0.02 vs shCON. Student's t test. n=30 neurons/3 experiments. Data are means, error bars represent SEM.

(F) Quantification of ADDL puncta intensity on GFP^+ or GFP^+ $PSD95^+$ regions of neurons following peptide incubation. * $p<0.004$ vs shCON. Student's t test. n= 30 neurons/3 experiments. Data are means, error bars represent SEM.

(G) 14 DIV primary hippocampal neuron cultures expressing indicated shRNAi and GFP were live-labeled with biotin-tagged ADDLs (250nM) and an anti-NgR1 antibody (1μg/μl), fixed and stained with secondary antibodies. Arrowheads mark ADDL/NgR1 costaining on GFP^+ dendrites. Scale bars=1μm. See also Table S1.

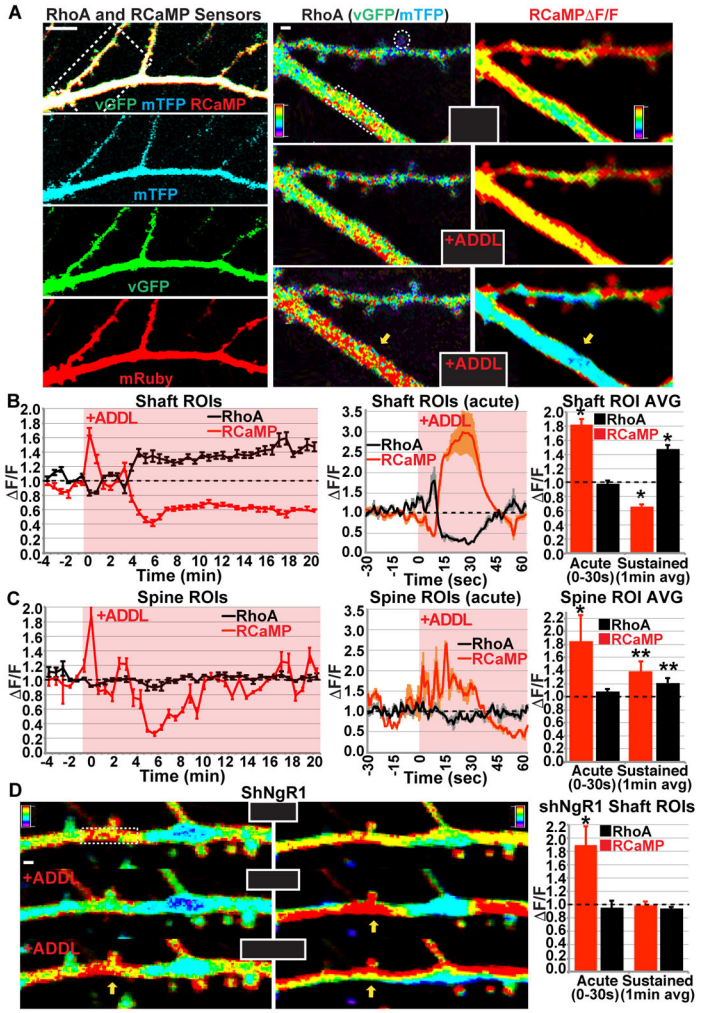

Fig. 4. ADDLs Activate RhoA and Inhibit Calcium Signaling in Dendrites Via NgR1

(A) (Left) Primary hippocampal neurons (14DIV) expressing RhoA2G FRET (mTFP/vGFP) and RCaMP (mRuby) sensors imaged live following exposure to ADDLs. RhoA (center) or RCaMP (right) sensor activity visualized in dendrites (boxed region in left panel) at the indicated times before and after ADDL (150nM) exposure. Example spine and shaft ROIs indicated, arrows highlight changes in RhoA and RCaMP activity. Scale bar=5μm (left panels) or 1μm (middle and right panels).

(B) (Left) Quantification of long-term RCaMP (red) and RhoA (black) sensor activity (ΔF/F) for shaft ROIs at indicated times following ADDL exposure to neuron above. Data points are means (30 seconds). n=8 shaft ROIs. (Middle) Quantification of acute sensor responses of shaft ROIs from neuron depicted above following ADDL exposure. n=8 shaft ROIs. (Right) Bars are maximum acute (30s mean) and sustained (1 min mean) sensor responses (ΔF/F) of shaft ROIs following ADDL exposure for all neurons analyzed. Error bars and shading represent SEM. n=7 neurons. *p<0.005 vs CON period (Student's t test).

(C) (Left) Quantification of long-term RCaMP (red) and RhoA (black) sensor activity (ΔF/F) for spine ROIs at indicated times following ADDL exposure for neuron depicted above. Data points are means (30 seconds). n=3 spine ROIs. (Middle) Quantification of

acute sensor responses of spine ROIs from neuron depicted above following ADDL exposure. n=3 spine ROIs. (Right) Bars are maximum acute (30s mean) and sustained (1 min mean) sensor responses (ΔF/F) of spine ROIs following ADDL exposure for all neurons analyzed. Error bars and shading represent SEM. n=6 neurons. **p<0.05 vs CON period (Student's t test).

(D) (Left) RhoA2G (left) and RCAMP (middle) expressing hippocampal neurons lacking NgR1 (shNgR1) show altered responses to ADDLs relative to control neurons (shCON) at indicated times. (Right) Bars are maximum acute (30s mean) and sustained (1 min mean) sensor responses (ΔF/F) of shaft ROIs following ADDL exposure for all neurons analyzed. Error bars represent SEM. n=6 neurons. *p<0.001 vs shCON period (Student's t test). See also Figure S4 and Table S1.

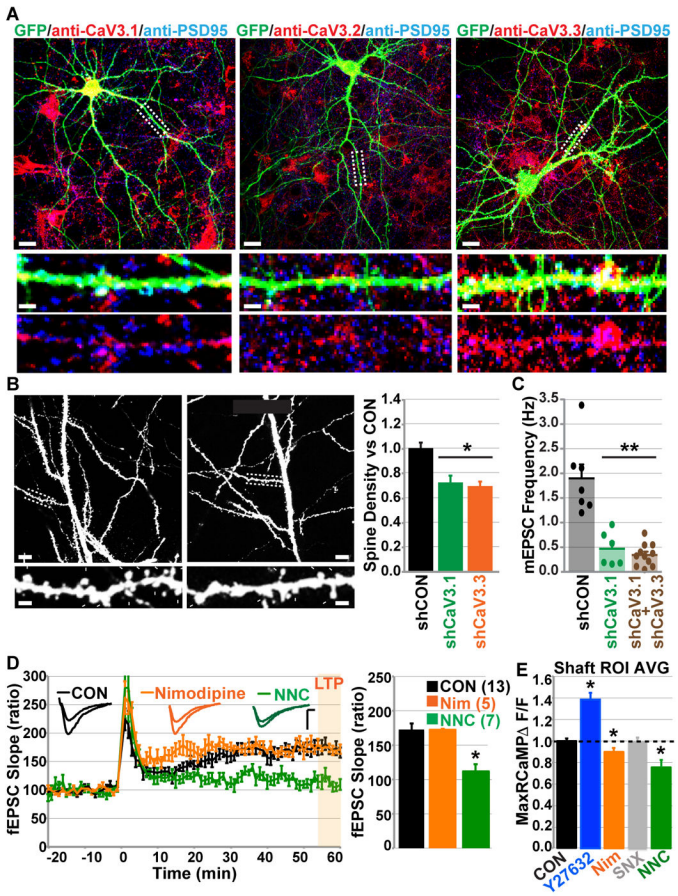

Fig. 5. T-Type Channels are Required for Synaptic Development, Plasticity and Calcium Signaling in Dendrites

(A) T-type calcium channels are expressed on dendrites during synaptic development. Cultured hippocampal neurons transfected with GFP, fixed and immunostained at 14 DIV with indicated antibodies. Arrows indicate T-type channel staining on dendrites. Scale bars=10 μm (top), 1 μm (below).

(B) RNAi targeting of CaV3.1 or CaV3.3 in hippocampal slice cultures reduces dendritic spine number. (Left) Representative CA1 pyramidal neurons shown, magnified image below (boxed region) illustrates spine loss. Scale bars=10μm (top), 1μm (below). (Right) Graph quantifies mean spine densities for noted conditions relative to CON (shCON). n=3 experiments. *p<0.04 vs shCON One-way ANOVA Dunnett's posthoc test. Error bars represent SEM.

(C) RNAi targeting of CaV3.1 alone or CaV3.1 and CaV3.3 in combination reduces mEPSC frequency in dissociated hippocampal neurons. Neurons transfected with GFP and shRNAis were recorded at 14–20 DIV. Bars indicate mean mEPSC frequency (hertz (Hz)). Error bars represent SEM. (n)=neurons indicated by circles. **p<0.0004 vs shCON One-way ANOVA Dunnett's posthoc test.

(D) (Left) T-type channel blocker NNC (10μM) but not L-type channel blocker Nimodipine (1μM) inhibits LTP from fEPSCs recordings of Schaffer collateral-CA1 synapses from acute mouse hippocampal slices (6 months). Example traces above (calibration 0.5mV, 5ms).

(right) Mean fEPSC 55–60 min post stimulation for indicated conditions. n in parentheses. *p<0.001 vs CON. One-way ANOVA Dunnett's posthoc test. Error bars represent SEM. (E) Graph illustrates maximum sustained (1 min mean) RCaMP sensor ΔF/F of shaft ROIs following exposure to indicated compounds (all 1μM). CON is DMSO (0.001%). n=3–11 neurons. *p<0.03 vs control imaging period (Student's t-test). Error bars represent SEM. See also Figure S5 and Table S1.

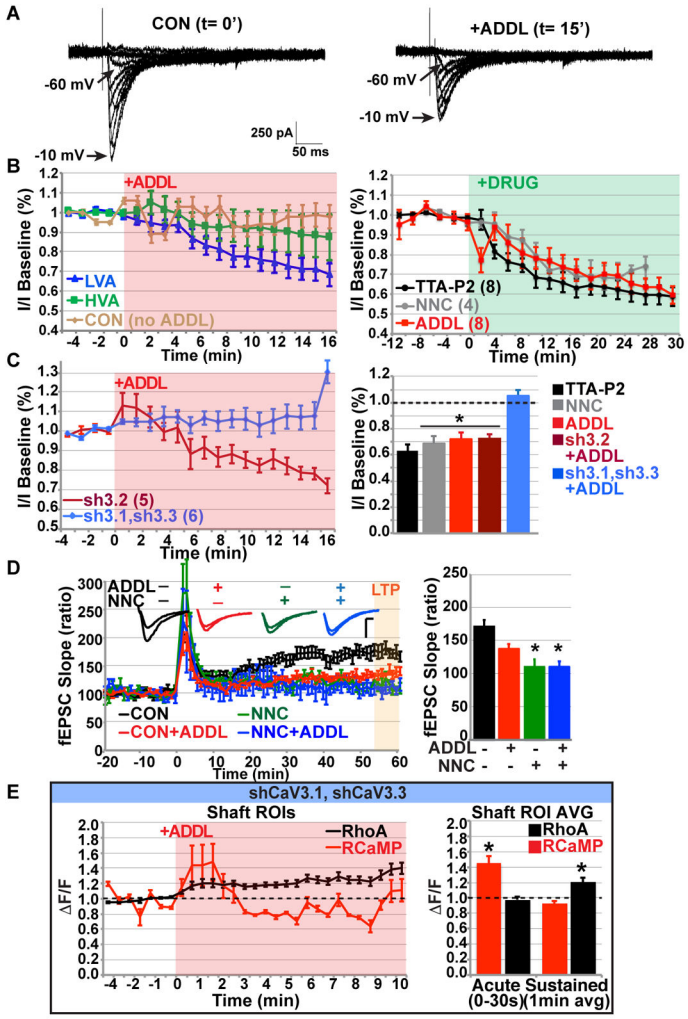

Fig. 6. ADDLs Block T-Type Channels Resulting in LTP Inhibition

A. T-type calcium channel currents are inhibited by ADDLs. Current recordings of T-type channels elicited from 14–18 DIV cultured hippocampal neurons by voltage step series (Fig. S6) at indicated times before (CON) and after ADDL exposure (150 nM).

B. (Left) Time course of current inhibition (current (I)/current baseline (I Baseline)) of low voltage activated (LVA), high voltage activated (HVA) currents following ADDL exposure (150 nM) or recordings under control conditions (CON no ADDL). (Right) Time course of T-type current inhibition following exposure to indicated drugs (1μM) or ADDL. n in parentheses.

C. (Left) Time course of T-type current inhibition of neurons expressing indicated shRNAis and GFP following exposure to ADDLs (150 nM). (right) Quantification of maximum mean inhibition for indicated conditions. n in parentheses. *p<0.02 vs CON period (Student's t test). Error bars represent SEM.

D. Combining ADDLs and T-type channel blocker NNC (10μM) inhibits LTP comparably to ADDLs or NNC alone. (left) fEPSC slopes recorded from acute mouse hippocampal slices (6 months) for indicated conditions. Example traces above (calibration 0.5mV, 5ms). (right) Mean fEPSC 55–60 min post stimulation for indicated conditions. n=6–8 animals/slices per

condition. *p<0.05 vs CON One-way ANOVA with Dunnett's posthoc test. Error bars represent SEM.

E. Hippocampal neurons expressing RhoA2G and RCaMP sensors and lacking CaV3.1 and 3.3 (shRNAi) show no calcium inhibition in response to ADDLs (150 nM). (Left) (Left) Quantification of RCaMP (red) and RhoA (black) sensor activity (ΔF/F) for shaft ROIs of shCaV3.1, shCaV3.3 expressing neuron following ADDL exposure at indicated times. Data are means (each 30 seconds), error bars represent SEM. n=8 shaft ROIs. (Right) Bars are maximum acute (30s mean) and sustained (1 min mean) sensor responses (ΔF/F) of shaft ROIs following ADDL exposure for all neurons analyzed. Error bars represent SEM. n=7 neurons. *p<0.01 vs CON period (Student's t test). See also Figure S6 and Table S1.

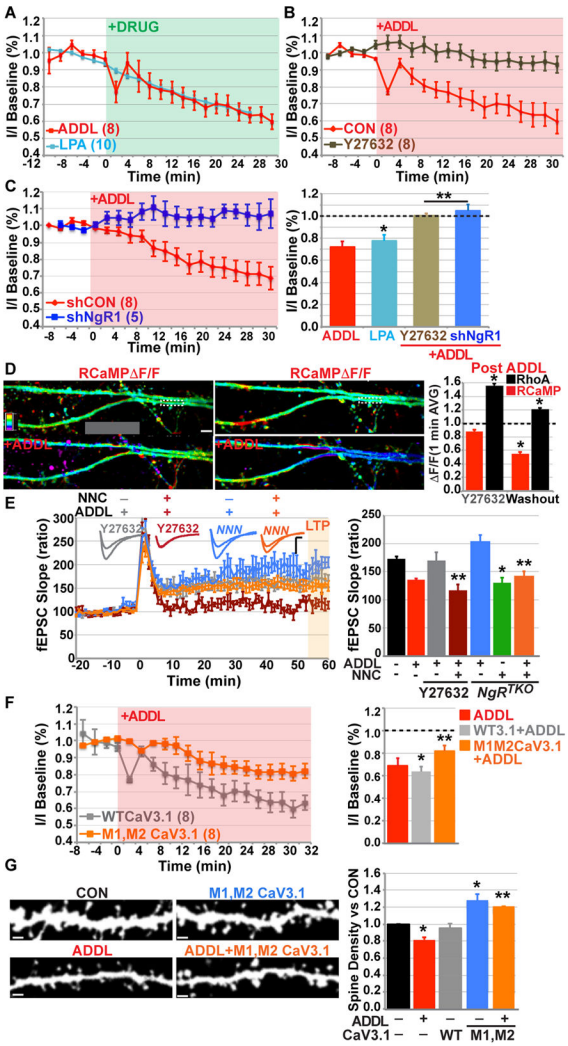

Fig. 7. ADDL-NgR Signaling Mediates ROCK Phosphorylation of Cav3.1 that Inhibits Calcium Signaling, LTP and Dendritic Spine Assembly

A. LPA (1μM) inhibits T-type currents (I)/(I Baseline) from cultured 14–18 DIV hippocampal neurons comparably to ADDLs (150nM). Error bars represent SEM. n in parentheses.

B. ROCK inhibition (Y27632-1μM) reverses ADDL's Inhibition of T-type currents (I)/(I Baseline). Error bars represent SEM. n in parentheses.

C. (Left) shRNAi-targeting of NgR1 reverses ADDL's inhibition of T-type currents (I)/(I Baseline) relative to shCON. Error bars represent SEM. (Right) Quantification of maximum mean inhibition for indicated conditions. n in parentheses. *p<0.01 vs CON period (Student's t test). **p<0.01 vs ADDL (Student's t test). Error bars represent SEM.

D. ROCK inhibition (Y27632-1μM) prevents ADDL inhibition of calcium activity (RCaMP) in dendrites of hippocampal neurons. (Left) Neuron expressing RCaMP and RhoA2G (not shown) sensors was incubated in Y27632 (1μM-10 minutes) and exposed to ADDLs (150nM) for indicated time. (Middle) Drug was washed out, cultured under control conditions (10 minutes) and exposed again to ADDLs (150nM) for the indicated time.

(Right) Quantification of maximum sustained ΔF/F (after ADDL addition) relative to control for indicated sensors and conditions. n=3 neurons. *p<0.001 vs CON (Student's t test).

E. T-type channel blocker NNC (10μM) reverses rescue of ADDL inhibition of LTP mediated by ROCK inhibition (Y27632-10μM) or NgR family knockout (NgR^{TKO}). (Left) fEPSC slopes recorded from acute mouse hippocampal slices (6 months) for indicated conditions. Example traces above (calibration 0.5mV, 5ms). (Right) Mean fEPSC 55–60 min post stimulation for indicated conditions. Error bars represent SEM. n in Table S1. *p<0.003 vs NgR^{TKO}, **p<0.04 vs ADDL + Y27632 or ADDL+ NgR^{TKO} respectively (Student's t test).

F. (Left) Overexpression of M1, M2 CaV3.1 mutant in cultured hippocampal neurons reverses ADDL's inhibition of T-type currents. Time course of T-type current inhibition (I)/(I Baseline) of neurons expressing indicated CaV3.1 isoforms and GFP following ADDL exposure (150nM). Error bars represent SEM. (Right) Quantification of maximum mean inhibition for indicated conditions. n in parentheses. *p<0.05 vs CON period (Student's t test). **p<0.02 vs WT3.1+ADDL (Student's t test). Error bars represent SEM.

G. (Left) M1, M2 CaV3.1 mutant reverses ADDL inhibition of dendritic spine number. CaV3.1 isoforms were coexpressed with GFP in hippocamapal slice cultures, exposed to ADDLs (150nM), fixed and stained. CA1 pyramidal neurons were imaged by confocal microscopy as illustrated. Arrowheads indicate mature dendritic spines. Scale bar=1μm. (Right). Quantification of dendritic spine density in indicated conditions below. Mean spine density expressed relative to control condition (vGFP alone). Error bars represent SEM. n=3 experiments. *p<0.05 vs CON. ** p<0.005 vs ADDL. One-way ANOVA Dunnet's post hoc test. See also Figure S7 and Table S1.

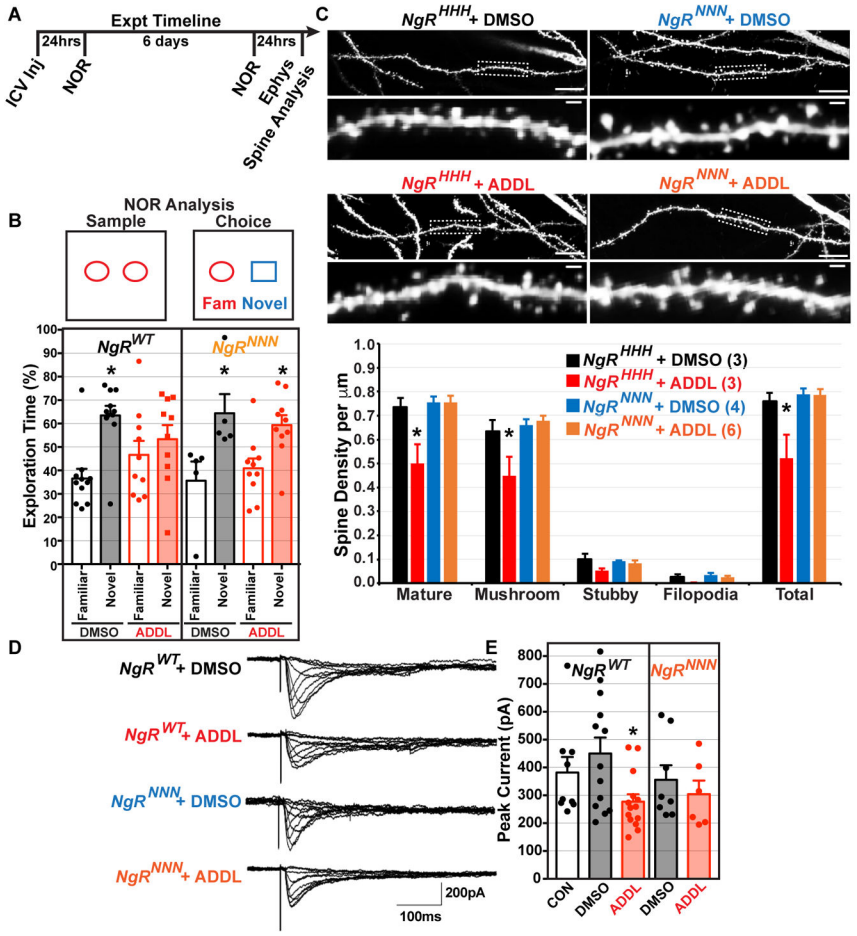

Fig. 8. ADDLs Block NOR Learning by NgR family Mediated Inhibition of Spine Assembly and T-Type Currents

A. Time line of ICV injections, NOR behavioral analysis, acute slice recordings and dendritic spine analysis.

B. ADDL-mediated deficits in novel object learning rescued by NgR family loss. (Top) Illustration of NOR sample and choice test with familiar (Fam) and novel (Nov) objections assessing two-hour retention memory. (Bottom) Quantification of exploration time with indicated objects following ICV injections with DMSO (0.8µls of 2%DMSO) or ADDLs (0.8µls of 50µM Aβ monomer equivalent). n= animals indicated by circles. Bars represent means, error bars SEM. *p<0.05 vs fixed 50% (chance) student's T test (see sup procedures for details).

C. ADDL-mediated reductions in dendritic spine density rescued by NgR family loss. (Top) Representative examples of proximal apical regions of GFP-positive CA1 pyramidal neurons from indicated *NgR* animals 8 days following ICV injections with indicated agents. Scale bar=10µm (Middle) Expanded boxed regions reveal mature dendritic spines (arrow heads). Scale bar=1µm. (Bottom) Quantification of mean dendritic spine density of different spine types for indicated genotypes and conditions. Error bars equal SEM. n=animal # in parentheses. *p<0.05 vs CON (NgR^{HHH} + DMSO) One-way ANOVA Dunnett's posthoc test.

D. ADDL-mediated inhibition of T-type currents rescued by NgR family loss. Representative T-type calcium channel currents elicited by voltage step series (see Fig. S6) from acute slice recordings of animals of indicated genotypes and conditions.

E. Mean peak current amplitude (pA) of T-type currents for indicated genotypes and conditions. Error bars equal SEM. n=animals indicated by circles. *p<0.03 vs CON *(NgR^{WT}* + DMSO) One-way ANOVA with Dunnett's posthoc test.

KEY RESOURCES TABLE

REAGENT or RESOURCE	SOURCE	IDENTIFIER
Antibodies		
Goat Polyclonal Anti-NgR1 antibody	R&D Systems	Cat#AF1440
Mouse Monoclonal Anti-PSD95 antibody	ThermoFisher	Cat#AB1543; RRID: AB_325399
Rabbit Polyclonal Anti-Synapsin antibody	Millipore	Cat#MA1-045; RRID: AB_2200400
Rabbit Polyclonal Anti-CaV3.1 antibody	Alomone Labs	Cat#ACC-021; RRID: AB_2039779
Rabbit Polyclonal Anti-Cav3.2 antibody	Alomone Labs	Cat#ACC-025; RRID: AB_2039781
Rabbit Polyclonal Anti-Cav3.3 antibody	Alomone Labs	Cat#ACC-009; RRID: AB_2039783
Chicken Polyclonal Anti-GFP antibody	Aves Labs	Cat#GFP-1020; RRID: AB_10000240
Biological Samples		
Chemicals, Peptides, and Recombinant Proteins		
Beta Amyloid Peptide 1-42 peptide (HFIP)	rPeptide	A-1163-2
Biotin-LC-Beta Amyloid Peptide 1-42 peptide (HFIP)	rPeptide	A-1118-1
NNC 55-0396	Tocris	2268
TTAP2	Alomone Labs	T-155
D-AP5	Tocris	0106
MNI-Caged L-Glutamate	Tocris	1490
LPA	Sigma	L7260
Y27632	Sigma	Y0503
C3 RhoA Inhibitor	Cytoskeleton Inc	Ct04
Nimodipine	Tocris	0600
SNX482	Tocris	2945
Conotoxin-MVIIC	Tocris	1084
Agatoxin-TK	Tocris	2802
TTX	Tocris	1078
CNQX	Tocris	1045
Experimental Models: Cell Lines		
Hamster: CHO cells	ATCC	CRL-11268
7PA2 CHO cells	Laboratory of Denis Selkoe	Podlisny et al., 1995
Homo sapien: HEK Cells	ATCC	CRL-3216
Experimental Models: Organisms/Strains		
mouse *NgR1; Rtn4r*^{tm1Matl}	MMRRC	011657
mouse *NgR2; Rtn4rl2*^{tm1Lex}	MGI	3609644

REAGENT or RESOURCE	SOURCE	IDENTIFIER
mouse *NgR3; Rtn4rl1*$^{Gt(OST188035)Lex}$	MGI	3609640
Tg(Thy1-EGFP)MJrs/J	The Jackson Laboratory	007788
3xTG-AD	The Jackson Laboratory	34830
Oligonucleotides		
Recombinant DNA		
pTriEXRhoA2G	Fritz et al., 2013	Addgene: 40176
pCAG-RCAMPh1	Laboratory of Loren Looger	Akerboom et al., 2013
pCMV-P50GAP and pCMV-DBK	Laboratory of Klaus Hahn	Pertz et al., 2003
pCMVCaV3.1^{M1+M2}	Laboratory of Terry Snutch	Iftinca et al., 2007
pCMVCaV3.1	Laboratory of Edward Perez-Reyes	Addgene: 45812
pCMVCaV3.2	Cribbs et al., 1998	Addgene: 45809
pCMVCaV3.3	Gomora et al., 2002	Addgene: 45810
shLuc (LL3.7)	Laboratory of Zachary Wills	Wills et al., 2012
shNgR1 (LL3.7)	Laboratory of Zachary Wills	Wills et al., 2012
pSYN-shCaV3.1	Laboratory of Daesoo Kim	Park et al., 2010
GIPZ-shCav3.2	Dharmacon	V3LMM_421392
GIPZ-shCav3.2	Dharmacon	V3LMM_421393
GIPZ-shCav3.3	Dharmacon	V2LMM_117677
GIPZ-shCav3.3	Dharmacon	V3LMM_466542
pDisplay-NgR1, NgR2 and NgR3	Laboratory of Zachary Wills	Wills et al., 2012
Software and Algorithms		
CalciumDetect	GitHub	https://github.com/zpwills/Zhao-et-al.-2017-Neuron-Paper
Open Field Analysis	Patel et al., 2014	http://www.seas.upenn.edu/~molneuro/autotyping.html